Corpora non agunt nisi fixata : ligand receptor binding kinetics in G protein-coupled receptors
Xia, L.

Citation
Xia, L. (2018, May 30). *Corpora non agunt nisi fixata : ligand receptor binding kinetics in G protein-coupled receptors*. Retrieved from https://hdl.handle.net/1887/62615

Cover Page

Universiteit Leiden

The handle http://hdl.handle.net/1887/62615 holds various files of this Leiden University dissertation.
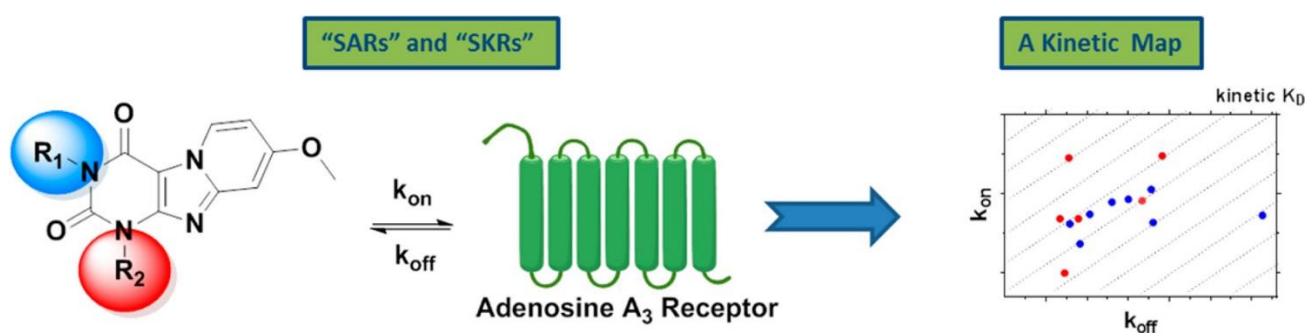
Author: Xia, L.
Title: Corpora non agunt nisi fixata : ligand receptor binding kinetics in G protein-coupled receptors
Issue Date: 2018-05-30

Chapter 4

Structure-Affinity Relationships and Structure-Kinetics Relationships of Pyrido[2,1-*f*]purine-2,4-dione Derivatives as Human Adenosine A$_3$ Receptor Antagonists

Lizi Xia, Wessel A. C. Burger, Jacobus P.D. van Veldhoven, Boaz J. Kuiper, Tirsa T. van Duijl, Eelke B. Lenselink, Ellen Paasman, Laura H. Heitman, and Adriaan P. IJzerman

About this chapter

We expanded on a series of pyrido[2,1-*f*]purine-2,4-dione derivatives as human adenosine A_3 receptor (hA_3R) antagonists to determine their kinetic profiles and affinities. Many compounds showed high affinities and a diverse range of kinetic profiles. We found hA_3R antagonists with very short residence time (RT) at the receptor (2.2 min for **5**) and much longer RTs (e.g. 376 min for **27**, or 391 min for **31**). Two representative antagonists (**5** and **27**) were tested in $[^{35}S]GTP\gamma S$ binding assays, and their RTs appeared correlated to their (in)surmountable antagonism. From a k_{on}-k_{off}-K_D kinetic map we divided the antagonists into three subgroups, providing a possible direction for the further development of hA_3R antagonists. Additionally, we performed a computational modelling study that sheds light on the crucial receptor interactions dictating the compounds' binding kinetics. Knowledge of target binding kinetics appears useful for developing and triaging new hA_3R antagonists in the early phase of drug discovery.

Introduction

The adenosine A_3 receptor is the youngest member discovered in the family of adenosine receptors,[1] all of which belong to class A G-protein coupled receptors (GPCR) and fall into four distinct subtypes (A_1, A_{2A}, A_{2B} and A_3). Although all subtypes are activated by the endogenous ligand adenosine, these purinergic receptors differ from each other in their distribution and to which G protein they are coupled. Following agonist activation, the A_1 and A_3 adenosine receptors cause a decrease in cAMP levels as they primarily couple to G_i proteins. The A_{2A} and A_{2B} adenosine receptors on the other hand, are primarily linked to G_s proteins and this leads to increased levels of cAMP upon receptor activation.[2]

Although the pharmacological characterization of adenosine receptors has been well documented,[3] the human adenosine A_3 receptor (hA_3R) is less well characterized because of its "dichotomy" in different therapeutic applications.[4] Moreover, certain ligands have been described as cytoprotective or cytotoxic merely depending on the concentration employed, highlighting the difficulties that arise when characterizing novel hA_3R compounds.[5] Nevertheless, there is no doubt that the hA_3R has therapeutic potential in clinical indications (i.e. cardiovascular diseases,[6, 7] cancer,[7, 8] and respiratory diseases[7, 9-11]), due to its overexpression on cancer and inflammatory cells.[3, 12-15]

Traditional drug screening methods, and those employed in previous hA_3R drug discovery attempts, revolve around the use of a ligand's affinity as the selection criterion for further optimization in a so-called structure-affinity relationships (SAR) approach. In recent years, however, there has been emerging the realization that selecting ligands based on their affinity, an equilibrium parameter, does not necessarily predict *in vivo* efficacy. This is due to the dynamic conditions *in vivo*, that often are in contrast to the equilibrium conditions applied in *in vitro* assays.[16] In fact a ligand's kinetic properties may provide a better indication of how a ligand will perform *in vivo*.[17] Specifically, the parameter of residence time (RT) has been proposed as a more relevant selecting criterion. The RT reflects the

121

lifetime of the ligand-receptor complex and can be calculated as the reciprocal of the ligand's dissociation constant (RT=1/k_{off}).[18, 19]

Table 1. Binding Affinity and Kinetic Parameters of 1-benzyl-8-methoxy-3-propylpyrido[2,1-f]purine-2,4(1H,3H)-dione[23, 24]
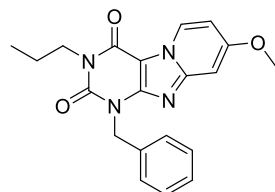
Compound	pK_i[a] ± SEM (mean K_i in nM)	KRI[b]	k_{on}[c] (M^{-1} s^{-1})	k_{off}[d] (s^{-1})	RT[e] (min)
1	8.5 ± 0.02 (3.2)	0.99 (0.97; 1.0)	(8.5 ± 1.2) x 10^5	(3.2 ± 0.02) x 10^{-4}	52 ± 0.3

[a] pK_i ± SEM (n ≥ 3, average K_i value in nM), obtained at 25 ^{o}C from radioligand binding assays with [^{3}H]PSB-11 ([^{3}H]**34**) on human Adenosine A_3 receptors stably expressed on CHO cell membranes.

[b] KRI (n = 2, individual estimates in parentheses), obtained at 10 ^{o}C from dual-point competition association assays with [^{3}H]**34** on human Adenosine A_3 receptors stably expressed on CHO cell membranes.

[c] k_{on} ± SEM (n ≥ 3), obtained at 10 ^{o}C from competition association assays with [^{3}H]**34** on human Adenosine A_3 receptors stably expressed on CHO cell membranes.

[d] k_{off} ± SEM (n ≥ 3), obtained at 10 ^{o}C from competition association assays with [^{3}H]**34** on human Adenosine A_3 receptors stably expressed on CHO cell membranes.

[e] RT (min) = 1/(60*k_{off}).

While the binding kinetics of some (labeled) hA$_3$R agonists have been studied,[20] this parameter has not been part of medicinal chemistry efforts for antagonists, i.e. yielding structure-kinetics relationships (SKR), next to SAR.[21] Therefore, in order to provide the first SKR analysis on the hA$_3$R, a highly potent and selective hA$_3$R antagonist scaffold was chosen. The pyrido[2,1-*f*]purine-2,4-dione template has been previously characterized with respect to affinity alone. In a Topliss approach[22] we had synthesized and characterized a number of highly potent and selective hA$_3$R antagonists.[23, 24] One of the reference antagonists (**1**) with good affinity and selectivity over other adenosine receptors is represented in **Table 1**. Using this compound as the starting point, we further selected and synthesized compounds to add to the library of pyrido[2,1-*f*]purine-2,4-dione derivatives. Using

radioligand displacement assays and competition association assays, we obtained affinity (K_i) and kinetic parameters (k_{on}, k_{off}, and RTs). This allowed a full SKR study alongside a more traditional SAR analysis. The findings provide information on the structural requirements for a favorable kinetic profile at the hA_3R and consequently may improve the *in vitro* to *in vivo* translation for hA_3R antagonists.

Results and discussion

Chemistry.

The synthesis approach shown in **Scheme 1** was adapted from Priego *et al.*[23, 24] Starting from the commercially available materials benzylurea (**3**), ethyl cyanoacetate and sodium methoxide 1-benzyl-6-amino-uracil (**4**) was synthesized in a 88% yield.[25] *In situ* dibromination of uracil **4** at the C^5 position by *N*-bromosuccinimide, followed by cyclisation with 4-methoxypyridine gave the pyrido[2,1-*f*]purine-2,4-dione (**5**) in a one pot reaction. Final compounds **1**, **2** and **6-22** (as depicted in Table 1) were obtained, with yields varying in the range of 3-86%, by alkylating the N^3 position of **5** using a variety of alkyl, alkenyl and alkynyl bromides in acetonitrile and 1,8-diazabicyclo[5.4.0]undec-7-ene (DBU) as a base. Secondly, to be able to diversify on the N^1 (R_2) position, building block **23** had to be obtained. Full conversion of methylcyclopropyl compound **2** into the desired debenzylated **23** was realized by multiple additions of ammonium formate and Pd(OH)$_2$ at 80 ^{o}C in ethanol overnight. Due to poor solubility **23** was extracted with hot DMF and Pd(OH)$_2$ was removed by filtration, resulting in a quantitative yield. Finally various N^1 substituted benzyl (**24**-**32**) and phenethyl (**33**) derivatives (**Scheme 1**) were made starting from the respective benzyl- or phenethyl bromides in DMF with K$_2$CO$_3$ used as base.

Biological Evaluation.

All binding affinities of the pyrido[2,1-*f*]purine-2,4-dione derivatives were determined at 25 ^{o}C in a 2 hours incubation protocol. All compounds were able to concentration-dependently inhibit specific

123

[3H]8-Ethyl-4-methyl-2-phenyl-(8R)-4,5,7,8-tetrahydro-1H- imidazo[2,1-i]-purin-5-one[26] ([3H]PSB-11, 34) binding to the human adenosine A_3 receptor and their affinities are listed in **Tables 1**, **2** and **3**. All compounds had (sub)nanomolar binding affinities ranging from 0.38 nM for compound **27** to 108 nM for compound **5**.

Scheme 1. Synthesis of 1,3-disubstituted-1H,3H-pyrido[2,1-f]purine-2,4-dione derivatives.
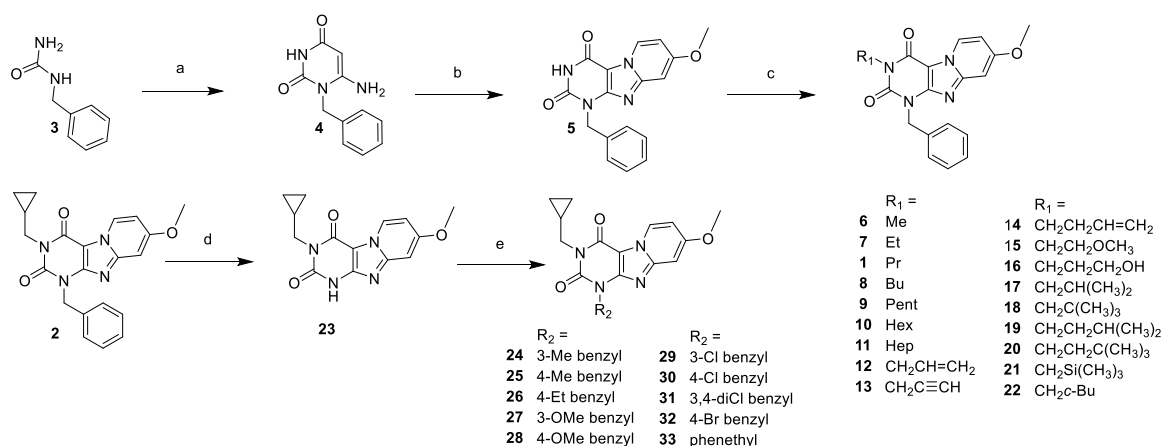
Reagents and conditions: **a**) ethyl cyanoacetate, NaOEt, EtOH, reflux, overnight; **b**) i) NBS, CH_3CN, 80 °C, 1h ii) 4-methoxypyridine, 80 °C, overnight; **c**) R_1-Br, DBU, CH_3CN, 80 °C, overnight; **d**) 20% $Pd(OH)_2$, ammonium formate, EtOH, reflux, overnight; **e**) R_2-Br, K_2CO_3, DMF, 40 °C overnight.

Subsequently, the human adenosine A_3 receptor ligands were screened in a so-called "dual-point" competition association assay,[27] allowing for the semi-quantitative estimation of the compounds' dissociation rates and therefore the compounds' RTs. The specific binding of [3H]**34** was measured after 20 and 240 minutes in the absence and presence of a single concentration (i.e. 1 x IC_{50}) of unlabeled human adenosine A_3 receptor antagonists, which yielded their Kinetic Rate Index (KRI). A long RT compound shows a characteristic "overshoot" followed by a steady decrease in specific binding until a new equilibrium is reached; in such a case the KRI value is greater than unity. Conversely, a ligand with a fast dissociation rate is represented by a more shallow curve, yielding a KRI value smaller than one when dividing the binding at t_1 by the binding at t_2. The KRI values in the series ranged from 0.38 to 4.06 (**Table 1**, **2** and **3**).

Table 2. Binding Affinities and Kinetic Parameters of Pyrido[2,1-*f*]purine-2,4-dione Derivatives with Modification on *N*-3 Position (R$_1$ group)
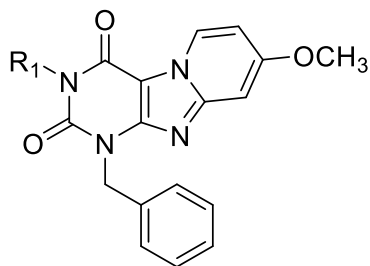
Compd.	R$_1$	pK_i[a] ± SEM (mean K$_i$ in nM)	KRI[b]	k_{on}[c] (M^{-1} s^{-1})	k_{off}[d] (s^{-1})	RT[e] (min)
5	H	7.0 ± 0.02 (108)	0.38 ± 0.12	(5.3 ± 1.5) x10^5	(1.4 ± 0.5) x 10^{-2}	2.2 ± 1.4
6	CH$_3$	7.7 ± 0.1 (20.8)	0.54 (0.52; 0.55)	n.d.[f]	n.d.	n.d.
7	CH$_2$CH$_3$	8.0 ± 0.1 (10.7)	0.80 (0.85; 0.75)	n.d.	n.d.	n.d.
8	CH$_2$CH$_2$CH$_2$CH$_3$	8.8 ± 0.1 (1.5)	1.29 (1.27; 1.31)	n.d.	n.d.	n .d.
9	CH$_2$CH$_2$CH$_2$CH$_2$CH$_3$	8.5 ± 0.02 (3.5)	1.11 (0.98; 1.24)	(1.1 ± 0.1) x 10^6	(6.0 ± 0.5) x 10^{-4}	28 ± 2.2
10	CH$_2$CH$_2$CH$_2$CH$_2$CH$_2$CH$_3$	8.6 ± 0.1 (2.8)	2.18 (2.15; 2.21)	(2.3 ± 1.0) x 10^5	(8.2 ± 1.3) x 10^{-5}	213 ± 35
11	CH$_2$CH$_2$CH$_2$CH$_2$CH$_2$CH$_2$CH$_3$	8.2 ± 0.2 (6.8)	4.06 (3.66; 4.46)	(4.2 ± 0.3) x 10^5	(6.2 ± 0.2) x 10^{-5}	278 ± 45
12	CH$_2$CH=CH$_2$	8.3 ± 0.1 (5.9)	0.72 (0.46; 0.99)	n.d.	n.d.	n.d.
13	CH$_2$C≡CH	8.4 ± 0.02 (4.3)	1.20 (1.16; 1.23)	n.d.	n.d.	n.d.
14	CH$_2$CH$_2$CH=CH$_2$	8.9 ± 0.1 (1.4)	1.23 (1.04; 1.41)	n.d.	n.d.	n.d.
15	CH$_2$CH$_2$OCH$_3$	7.7 ± 0.2 (23)	0.70 (0.70; 0.70)	(4.3 ± 0.8) x 10^5	(6.3 ± 0.7) x 10^{-4}	27 ± 2.6
16	CH$_2$CH$_2$CH$_2$OH	7.1 ± 0.1 (81)	1.04 ± 0.11	n.d.	n.d.	n.d.
17	CH$_2$CH(CH$_3$)$_2$	8.9 ± 0.02 (1.2)	1.64 ± 0.24	(7.8 ± 2.7) x 10^5	(2.0 ± 0.8) x 10^{-4}	148 ± 102
18	CH$_2$C(CH$_3$)$_3$	8.5 ± 0.1 (3.5)	1.73 ± 0.28	(5.5 ± 1.3) x 10^5	(1.1 ± 0.4) x 10^{-4}	250 ± 147
19	CH$_2$CH$_2$CH(CH$_3$)$_2$	8.5 ± 0.04 (3.5)	1.39 (1.23; 1.55)	n.d.	n.d.	n.d.
20	CH$_2$CH$_2$C(CH$_3$)$_3$	8.1 ± 0.02 (8.0)	0.95 (1.02; 0.87)	n.d.	n.d.	n.d.
21	CH$_2$Si(CH$_3$)$_3$	8.6 ± 0.03 (2.7)	1.36 (1.26; 1.45)	n.d.	n.d.	n.d.
2	CH$_2$C$_3$H$_5$	9.0 ± 0.02 (1.0)	2.68 ± 0.48	(2.8 ± 0.5) x 10^6	(6.0 ± 1.7) x 10^{-5}	315 ± 105
22	CH$_2$C$_4$H$_7$	8.6 ± 0.03 (2.7)	1.48 (1.66;1.30)	n.d.	n.d.	n.d.

Compounds with a KRI value less than 0.7 or greater than 1.5 were selected for complete kinetic characterization through the use of a competition association assay with [^{3}H]**34** (**Figure 1A**). In order to obtain extensive Structure-Kinetics Relationships (SKR), close structural analogs (**9**, **28**, **29** and **30**) of **1** were also tested to obtain their association (k$_{on}$) and dissociation (k$_{off}$) rate constants. Association rate constants varied by 30-fold, ranging from (1.0 ± 0.1) x 10^5 M^{-1}s^{-1} for antagonist **31** to (3.0 ± 0.3) x 10^6 M^{-1}s^{-1} for antagonist **30** (**Table 3**).

Interestingly, there was an approximately 290-fold difference in dissociation rate constants, reflecting the divergent KRI values. Antagonist **5** had the fastest dissociation rate constant of (1.4 ± 0.5) x 10^{-2} s^{-1} and thus the shortest RT of 2.2 min, while both antagonist **27** and **31** had the slowest dissociation rate constants of (4.7 ± 0.7) x 10^{-5} s^{-1} and (5.3 ± 1.5) x 10^{-5} s^{-1}, respectively, and thus the longest RTs of 376 min and 391 min, respectively. Of note, the long RT antagonist **27** (**Figure 1A**)

Table 3. Binding Affinities and Kinetic Parameters of Pyrido[2,1-*f*]purine-2,4-dione Derivatives with Modification at R$_2$
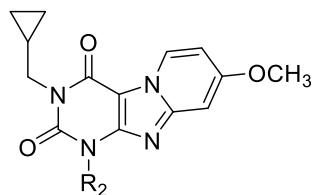
Compd.	R$_2$	pK_i[a] ± SEM (mean K_i in nM)	KRI[b]	k_{on}[c] (M^{-1} s^{-1})	k_{off}[d] (s^{-1})	RT[e] (min)
2	benzyl	9.0 ± 0.02 (1.0)	2.68 ± 0.48	(2.8 ± 0.5) x 10^6	(6.0 ± 1.7) x 10^{-5}	315 ± 105
24	3-CH$_3$-benzyl	8.8 ± 0.02 (1.5)	1.18 (1.18; 1.17)	n.d.[f]	n.d.	n.d.
25	4-CH$_3$-benzyl	9.0 ± 0.1 (0.92)	1.15 (1.03; 1.27)	n.d.	n.d.	n.d.
26	4-CH$_2$CH$_3$-benzyl	9.2 ± 0.04 (0.71)	0.81 (0.82; 0.79)	n.d.	n.d.	n.d.
27	3-OCH$_3$-benzyl	9.4 ± 0.03 (0.38)	2.24 (2.32; 2.15)	(4.8 ± 0.2) x 10^5	(4.7 ± 0.7)x 10^{-5}	376 ± 58
28	4-OCH$_3$-benzyl	8.9 ± 0.01 (1.4)	1.39 (1.22; 1.55)	(4.8 ± 0.1) x 10^5	(7.8 ± 2.0) x 10^{-5}	250 ± 72
29	3-Cl-benzyl	8.3 ± 0.02 (4.9)	0.89 (1.06; 0.72)	(8.2 ± 1.3) x 10^5	(4.7 ± 0.7) x 10^{-4}	36 ± 5.5
30	4-Cl-benzyl	8.9 ± 0.01 (1.2)	1.11 (1.02; 1.20)	(3.0 ± 0.3) x 10^6	(8.2 ± 0.2) x 10^{-4}	20 ± 0.5
31	3,4-dichlorobenzyl	8.3 ± 0.01 (5.3)	3.12 (3.49; 2.75)	(1.0 ± 0.1) x 10^5	(5.3 ± 1.5) x 10^{-5}	391 ± 137
32	4-Br-benzyl	8.9 ± 0.1 (1.2)	1.19 (1.30; 1.08)	n.d.	n.d.	n.d.
33	phenethyl	8.1 ± 0.04 (7.7)	1.09 (1.21; 0.97)	n.d.	n.d.	n.d.

[a] pK_i ± SEM (n ≥ 3, average K_i value in nM), obtained at 25 °C from radioligand binding assays with [^{3}H]**34** on human Adenosine A$_3$ receptors stably expressed on CHO cell membranes.

[b] KRI ± SEM (n = 3) or KRI (n = 2, individual estimates in parentheses), obtained at 10 °C from dual-point competition association assays with [^{3}H]**34** on human Adenosine A$_3$ receptors stably expressed on CHO cell membranes.

[c] k_{on} ± SEM (n ≥ 3), obtained at 10 °C from competition association assays with [^{3}H]**34** on human Adenosine A$_3$ receptors stably expressed on CHO cell membranes.

[d] k_{off} ± SEM (n ≥ 3), obtained at 10 °C from competition association assays with [^{3}H]**34** on human Adenosine A$_3$ receptors stably expressed on CHO cell membranes.

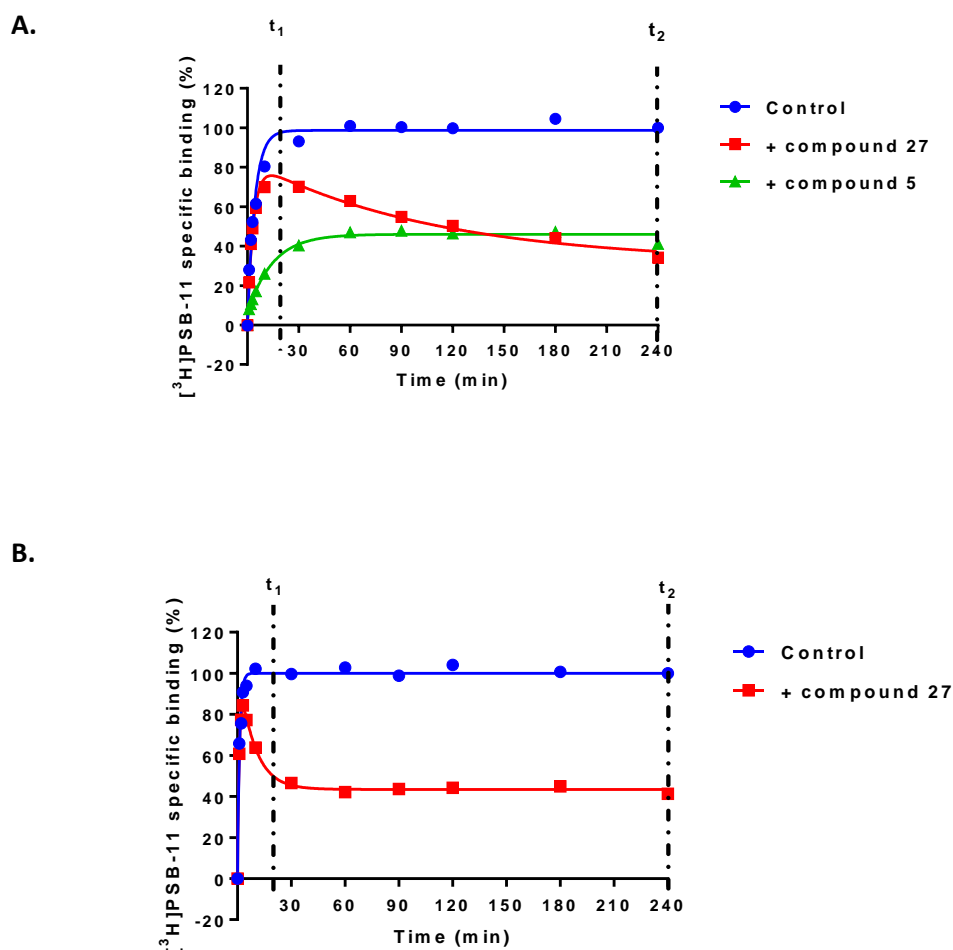[e] RT (min) = $1/(60*k_{off})$

[f] n.d. = not determined.

Figure 1: (**A**) Representative competition association assay curves of [^{3}H]**34** in the absence (control) or presence of a long residence time compound **27** and a short residence time compound **5**. Experiments were performed at 10 °C using the compound's respective IC$_{50}$ value at the hA$_3$R. (**B**) Competition association curves of [^{3}H]**34** in the absence (control) or presence of long residence time compound **27**. Experiments were performed at 25 °C using the compound's respective IC$_{50}$ value at the hA$_3$R. t$_1$ is the radioligand binding at 20 min, while t$_2$ is the radioligand binding at 240 min.

displayed a typical "overshoot" in the competition association curve, indicative of a slower

dissociation than the radiolabeled probe [^{3}H]**34,** while the short RT antagonists, exemplified by

antagonist **5** (**Figure 1A**) presented more shallow, gradually ascending curves. There was a good

correlation between the negative logarithm of the antagonists' dissociation rate constants and their

KRI values derived from the kinetic screen (**Figure 2A**), which confirmed that a compound's KRI value

is a good predictor for its dissociation rate constant. Notably, the experimental temperatures in the kinetic assays were lower than in the equilibrium displacement assays (25 $^{\circ}$C vs 10 $^{\circ}$C), because kinetic studies performed at 25 $^{\circ}$C were compromised by the nature of the compounds tested. This is shown in **Figure 1B**, where the "overshoot" of long RT antagonist **27** happened before the t_1 checkpoint of 20 min, which did not happen at 10 $^{\circ}$C. A significant correlation was also observed between the antagonist affinities (K_i values) determined in equilibrium displacement experiments and their kinetic K_D values derived from competition association experiments (**Figure 2B**), despite the differences in assay temperature (25 $^{\circ}$C vs 10 $^{\circ}$C). Interestingly, the kinetic association rate constants (k_{on}) did not show any significant correlation with affinity (**Figure 2C**), whilst the dissociation rate constants (k_{off}) had a fair correlation with affinity (**Figure 2D**).

The representative long RT and short RT antagonists (**27** and **5**) were selective for the hA$_3$ receptor when compared to other adenosine receptors (i.e. human adenosine A$_1$ and A$_{2A}$ receptor, **Table S1**). These two antagonists (**27** and **5**) with comparable association rate constants but distinct dissociation rate constants (or RTs) were further analyzed in a [^{35}S]GTPγS binding assay in which we studied the (in)surmountable antagonism induced by the two compounds (**Figure 3**).

Moreover, a k_{on}-k_{off}-K_D "kinetic map" (**Figure 4**) was constructed based on the compounds' divergent affinities (expressed as kinetic K_D values) and kinetics parameters, yielding a division of these antagonists into three different sub-categories: antagonists that show similar k_{off} values (< 2-fold) but due to differing k_{on} values (> 28-fold) have different K_D values (~100-fold, Group A); antagonists that display similar K_D values (< 10-fold) despite showing divergent k_{off} and k_{on} values (17-fold and 30-fold, Group B); antagonists with similar k_{on} values (< 5-fold), but due to differing k_{off} values (~290-fold) have different K_D values (> 110-fold, Group C). Additionally, we applied molecular modeling to compare the binding behavior in some molecular detail of several antagonists with similar affinities (**2** vs **10**; **31** vs **29** or **30**) (**Figure 5**).
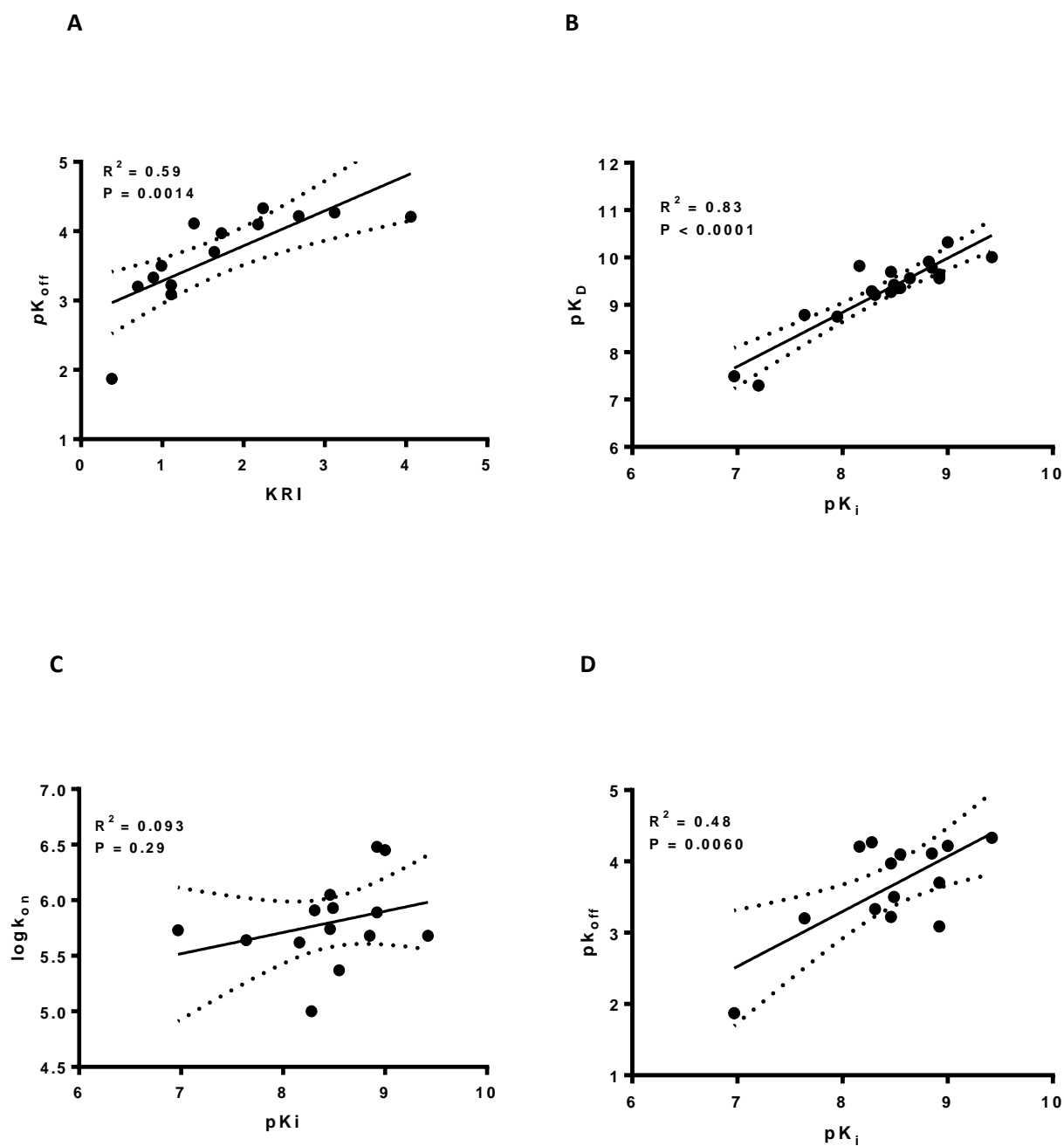
Figure 2: The correlations between the negative logarithm of the human adenosine A_3 receptor antagonists' dissociation rates (pk_{off}) and their kinetic rate index (KRI) (**A**), the human adenosine A_3 receptor antagonists' affinity (pK_i) and their "kinetic K_D" (pK_D) (**B**), association rate constants ($logk_{on}$) (**C**), dissociation rate constants (pk_{off}) (**D**). The central line corresponds to the linear regression of the data, the dotted lines represent the 95% confidence intervals for the regression. Data used in these plots are detailed in **Tables 1** - **3**. Data are expressed as mean from at least three independent experiments.

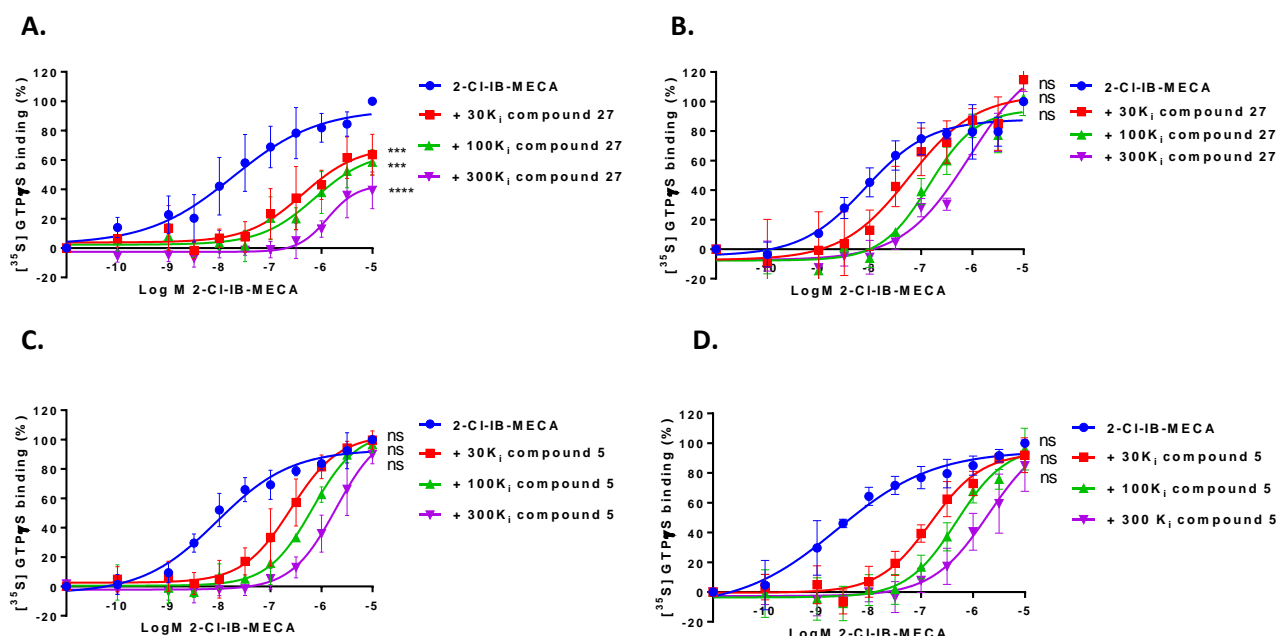**Figure 3:** 2-Cl-IB-MECA-stimulated [^{35}S] GTPγS binding to hA$_3$R stably expressed on CHO cell membranes (25 °C) in the absence or presence of long-residence-time antagonist **27** (**A** and **B**, normalized and combined, n ≥3), or short-residence-time antagonist **5** (**C** and **D**, normalized and combined, n ≥3). Antagonist **27** (**A**), **5** (**C**) were incubated for 60 min prior to the challenge of the hA$_3$R agonist 2-Cl-IB-MECA, at a concentration ranging from 0.1 nM to 10 μM, for another 30 min. Antagonist **27** (**B**), **5** (**D**) were coincubated with 2-Cl-IB-MECA, at the same concentration range, for 30 min. The agonist curves were generated in the presence of increasing concentrations of antagonists, namely 30-, 100-, 300-fold their respective K$_i$ values. Curves were fitted to a four parameter logistic dose-response equation. Data is from at least three independent experiments performed in duplicate, normalized according to the maximal response (100%) produced by 2-Cl-IB-MECA alone. The shift in agonist EC$_{50}$ values was determined to perform Schild analyses. Two-way ANOVA with Dunnett's post-test was applied for the comparison of E$_{max}$ by agonist control, * $p < 0.05$, ** $p < 0.01$, *** $p < 0.001$, **** $p < 0.0001$, **** $p < 0.0001$, ns for not significant.

Structure-Affinity Relationships (SAR) and Structure-Kinetics relationships (SKR).

According to previous studies from our group,[23, 24] methoxy-substitution at the C^8 position (**Table 1**) of the pyrido[2,1-*f*]purine-2,4-dione scaffold yielded selective hA$_3$R antagonists with good affinity (3.2 nM for **1** as a reference compound). From our preliminary studies, this methoxy-group appeared important for slow dissociation (**1** vs Compound **S2** from **Figure S1**, **Table S2**). Due to the nanomolar affinity and close-to-unity KRI value of **1**, it was treated as the starting point of this SAR and SKR study, having, on further analysis, an association rate constant of (8.5 ± 1.2) x 10^5 M^{-1}s^{-1} and a

131

dissociation rate constant of $(3.2 \pm 0.02) \times 10^{-4}$ s^{-1} (RT = 52 min). Next, we decided to investigate R_1 substitutions (**Table 2**), beginning with antagonist **5** (R_1 = H).

*The substitutions at R_1 (**Table 2**).*

Firstly, an increase in alkyl chain length was investigated, indicating an elongated carbon chain had a cumulative effect on KRI (**5**, **6**, **7**, **8**, **10**, **11)**, with the exception of antagonist **9** (KRI values from 0.38 to 4.06). One could point to a possible correlation between lipophilicities and dissociation rate constants (and consequently RTs) to explain this trend (**Figure S2A**). However, with all of the antagonists kinetically characterized, no such correlation was observed (**Figure S2B**). Therefore other reasons should be taken into account as to why elongating the carbon chain has such a profound effect on the ligand's dissociation rate. The role of membrane-drug interactions in determining the pharmacological profile is a possible reason, especially the role long carbon tails have in such interactions.[28] Interesting to point out is the affinity of antagonist **11** which, had a traditional lead selection process taken place, would most likely have resulted in the elimination of this compound due the more favorable affinity and hydrophilic properties of its shorter carbon chain counterparts (**8** or **9**) (affinities: 6.8 nM vs 1.5 nM or 3.5 nM, KRI values: 4.06 vs 1.29 or 1.11). This would have overlooked the efficacy this compound could offer due to its longer residence time.

Secondly, the presence of a more rigid substitution of the R_1 group of saturated equivalents (antagonists **1** and **8)** led to antagonists **12** and **14**, with similar improvement in the affinity pairs (**12** and **14**: 5.9 nM and 1.4 nM; **1** and **8**: 3.2 nM and 1.5 nM) and KRI values (**12** and **14**: 0.72 and 1.23; **1** and **8**: 0.99 and 1.29). Further rigidification with alkyne (**13**) rather than alkene **(12)** maintained affinities (4.3 nM vs 5.9 nM) and increased KRI values (1.20 vs 0.72). This alkyne could be the starting point for a further study on "click-chemistry" for introducing e.g., fluorescent tags.[29-31]

Thirdly, the introduction of a polar atom or group in antagonist **15** or **16**, respectively, led to a decrease in affinity compared to their non-polar counterpart **1** (23 nM or 81 nM vs 3.2 nM). The

132

changes in KRI values between antagonist **1** and its polar counterparts **15** and **16** can be considered minor (0.99 vs 0.70 and 1.04). Of note, by comparing affinities and kinetic profiles of polar antagonist **15** with its non-polar equivalent **1**, we found the polarity at the "lipophilic carbon chain" resulted in slower association (k_{on} of (4.3 ± 0.8) x 10^5 $M^{-1}s^{-1}$ vs (8.5 ± 1.2) x 10^5 $M^{-1}s^{-1}$) but faster dissociation (k_{off} of (6.3 ± 0.7) x 10^{-4} s^{-1} vs (3.2 ± 0.02) x 10^{-4} s^{-1}), with a concomitant decrease in affinity (23 nM vs 3.2 nM).

Moreover, the bulkiness of the substituents was studied with branched carbon side chains (**17, 18, 19, 20** and **21**) or aliphatic rings (**2** and **22**). As to the branched carbon side chains, compound affinities remained in the nanomolar range, while in terms of KRI values, 2-carbon-linker branched side chains (**17** and **18**) caused larger KRI values than those of either their linear counterparts (**8** and **9**) or 3-carbon-linear branched side chains (**19** and **20**) (**17**: 1.64 vs 1.29 or 1.39; **18**: 1.73 vs 1.11 or 0.95). Although the association rate constants of **17** and **18** were similar to other antagonists in Table 2, the dissociation rate constants suggest their branched side chains have an extra "anchoring" effect, compared with the linear counterparts. For example, the k_{off} of **18** with a 5-carbon branched side chain was quite similar to **10** or **11** having a 6 or 7-carbon linear side chain ((1.1 ± 0.4) x 10^{-4} s^{-1} vs (8.2 ± 1.3) x 10^{-5} s^{-1} or (6.2 ± 0.2) x 10^{-5} s^{-1}). The presence of a slightly less polar but larger silicon atom (**21**) instead of carbon (**18**) made the KRI value decrease (1.36 vs 1.73), although the affinity remained virtually the same (2.7 nM vs 3.5 nM).

Interestingly, another reported analogue (**2**)[23] of compound **1**, with cyclopropylmethyl substitution at the R_1 group, led to unique kinetic parameters, i.e. a combination of a fast association rate constant ((2.8 ± 0.5) x 10^6 $M^{-1}s^{-1}$ vs (8.5 ± 1.2) x 10^5 $M^{-1}s^{-1}$) and a slow dissociation rate constant ((6.0 ± 1.7) x 10^{-5} s^{-1} vs (3.2 ± 0.02) x 10^{-4} s^{-1}), although the affinities of **2** and **1** were similar (1.0 ± 0.03 nM vs 3.2 ± 0.1 nM, respectively). The RT of compound **2** was the longest in **Table 2** with 315 min. For the antagonist with cyclobutylmethyl (**22**), affinity (2.7 nM vs 1.0 nM) and KRI value (1.48 vs 2.68) were lower than for compound **2**.

Although the dissociation rate constants of the antagonists in **Table 2** varied greatly depending on the R_1 substituent, the association rate constants were more similar (within 5-fold). Association rate constants are often reasoned to be caused by a diffusion limited process whereby the collision rate of ligand and receptor determines the rate of ligand-receptor complex formation.[32] When no conformational changes are required for the receptor and ligand to bind and when taking into account the proportion of the receptor responsible for binding, this sets the association rate constant at observed limits of around 10^7 $M^{-1}s^{-1}$.[33] As the association rate constants for all R_1 substituted compounds were slower than the diffusion limit by at least 3.5 fold (**2**), we hypothesize target engagement for R_1 substituted antagonists is more hampered than imposed by the diffusion limit.

*The substitutions at R_2-group (**Table 3**).*

From **Table 2** we learned that cyclopropylmethyl-substituted antagonist **2** exhibited a kinetic profile as a long RT compound whilst showing the affinity previously reported.[23] As a result, this compound became the starting point for our exploration of the substitutions (*R_2-group*) on the aromatic ring.

Introduction of a non-polar alkyl substituent on antagonist **2**'s benzyl ring (**24, 25, 26**), resulted in a decrease in KRI values (from 2.68 to 0.81), while slight variations in affinity were observed. Then, introduction of a polar methoxy substituent on antagonist **2**'s benzyl ring, led to mixed results with a small decrease in RT at *para*-position, and a slight increase in RT at *meta*-position in **28** (250 min vs 315 min) and **27** (376 min vs 315 min), respectively. In particular, the long residence time for **27** in combination with its sub-nanomolar affinity (0.38 nM), made this compound stand out in the series.

Next, halogen substitutions on antagonist **2**'s benzyl ring were examined. Apparently, the position of halogen substitution is important for affinity as *para*-substitution in antagonist **30** and **32** yielded similar affinity compared to **2** (1.2 nM vs 1.2 nM vs 1.0 nM). The one compound with *meta*-substitution, **29,** showed a 5-fold decrease in affinity compared to **2** (4.9 nM vs 1.0 nM). Dichloro-
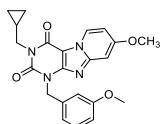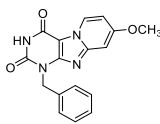
substituted compound **31** had the largest KRI value (3.12) among the halogen-substituted antagonists; the *para*-bromo substituted compound **32** was similar in this respect to *para*-chloro substituted **30** (1.19 vs 1.11). In a full competition association experiment we determined the rate constants for **31**, and learned it had the longest RT of all compounds kinetically characterized (391 min), concomitant with the slowest association rate constant of the compounds kinetically characterized ($(1.0 \pm 0.1) \times 10^5$ $M^{-1}s^{-1}$). Previous theoretical studies have indicated the strength of halogen bonding can be increased through the introduction of electron withdrawing groups onto halobenzenes.[34] Such would be the case for **31** where the additional chloro substituent forms a stronger halogen bonding interaction with the R_2 binding pocket. Introducing a phenethyl (**33**) rather than benzyl substituent (**2**) led to a decrease in affinity (7.7 nM vs 1.0 nM), whilst the KRI value was also strongly affected (1.09 vs 2.68). This observation parallels our previous findings that the binding pocket for the R_2 substituent is of limited size.[23]

Functional Assay.

Following kinetic characterization, a long (**27**) and a short (**5**) RT compound were chosen for functional characterization in a [^{35}S]GTPγS binding assay, also because for these two compounds the k_{on} values were similar ($(4.8 \pm 0.2) \times 10^5$ $M^{-1}s^{-1}$ vs $(5.3 \pm 1.5) \times 10^5$ $M^{-1}s^{-1}$). This difference allowed a possible link to be made between RTs and efficacies.

Pretreatment of hA_3 receptor membranes with increasing concentrations of the long RT antagonist **27**, before stimulation by the A_3 receptor agonist 2-Cl-IB-MECA, induced insurmountable antagonism. In other words, the 2-Cl-IB-MECA concentration-effect curves were shifted to the right with a concomitant decrease in the maximal response (**Figure 3A**). Conversely, the short RT antagonist **5** displayed surmountable antagonism, shifting 2-Cl-IB-MECA's curves to the right without affecting its maximum effect (**Figure 3B**).

Table 4. Functional activity of hA$_3$ receptor antagonists from [^{35}S]GTPγS binding assays

Ligands	Preincubation			Coincubation		Mode of antagonism
	RT^a (min)	pA$_2$^{b}	Schild slope^b	pA$_2$^{b}	Schild slope^b	
27	376 ± 58	N.A.^{c}	N.A.	8.9 ± 0.3	0.9 ± 0.2	Competitive insurmountability
5	2.2 ± 1.4	6.8 ± 0.4	1.0 ± 0.3	7.2 ± 0.4	1.0 ± 0.2	Competitive surmountability

^{a} RTs were obtained from Tables **1** and **2**.

^{b} Obtained from Schild analyses.

^{c} N.A.: not applicable.

In this experimental set-up, the Schild-slope of **5** generated from Schild-plots was close to unity (**Table 4**), and the compound's pA$_2$ value was comparable with its pK$_i$ value (6.8 ± 0.4 vs 7.0 ± 0.02). We also performed co-incubation experiments with these antagonists in the presence of 2-Cl-IB-MECA. In this experimental set-up, all antagonists produced a rightward shift of the 2-Cl-IB-MECA concentration-effect curves without a suppression of the maximal response (**Figure 3C** and **D**). Notably, the Schild-slopes of both long and short RT antagonists (**27** and **5**) were close to unity (0.9 ± 0.2 for **27**, 1.0 ± 0.2 for **5**, **Table 4**). In addition, the pA$_2$ value of **5** was comparable with the result from the pre-incubation condition (7.2 ± 0.4 vs 6.8 ± 0.4, **Table 4**), and the pA$_2$ value of **27** was also in agreement with its pK$_i$ value (8.9 ± 0.3 vs 9.4 ± 0.03).

Kinetic Map.

Using the association (k_{on}) and dissociation (k_{off}) rate constants obtained from competition association experiments (**Tables 1**-**3**), a kinetic map (**Figure 4**) was constructed by plotting these values on the *y*-axis and *x*-axis, respectively. The dashed diagonal parallel lines represent the kinetically derived K_D values ($K_D = k_{off}/k_{on}$). Out of this map three subgroups emerged. Group A represents compounds that exhibit similar k_{off} values, but with vastly different k_{on} values. As a consequence a diverse range of K_D values was observed. Previous SKR studies have primarily focused on optimizing dissociation rates and RTs for predicting *in-vivo* efficacy and creating a kinetically favorable ligand. Yet recently, there has been greater acknowledgment of the important role that the association rate constants may play in determining the efficacy of a drug as the result of increased rebinding or increased drug-target selectivity.[19] A kinetic map would thus allow for the selection of compounds with appropriate RTs whilst exploring the role of association rate constants in determining efficacy by choosing a rapidly or slowly associating compound, i.e. **2** or **31** ((2.8 ± 0.5) x 10^6 $M^{-1}s^{-1}$ vs (1.0 ± 0.1) x 10^5 $M^{-1}s^{-1}$). Group B displays ligands that exhibit a narrow range of affinity (K_D: 0.1 nM - 1 nM), yet a wide range of k_{off} values that result in RTs ranging from 20 min to 391 min. This information would have gone unnoticed in a traditional SAR hit-to-lead approach and would most likely have led to the selection of high affinity compounds not in possession of a potentially efficacy promoting long residence time. Thus, combining SAR with SKR aspects in lead optimization would allow the selection of not only potent but also long RT compounds through the drug development pipeline. Lastly group C represents compounds that present similar k_{on} values but due to differing k_{off} values show considerable differences in affinities (K_D). This illustrates the differences that were observed in the binding kinetics of the R_1 and R_2 substituents, as group C mainly consists of R_1 substituents (non-cyclopropylmethyl substituents), whilst group A mainly consists of R_2 substituents (cyclopropylmethyl substituents). This difference also suggests a different mode of receptor-ligand interaction during the binding process of the two ligand groups.
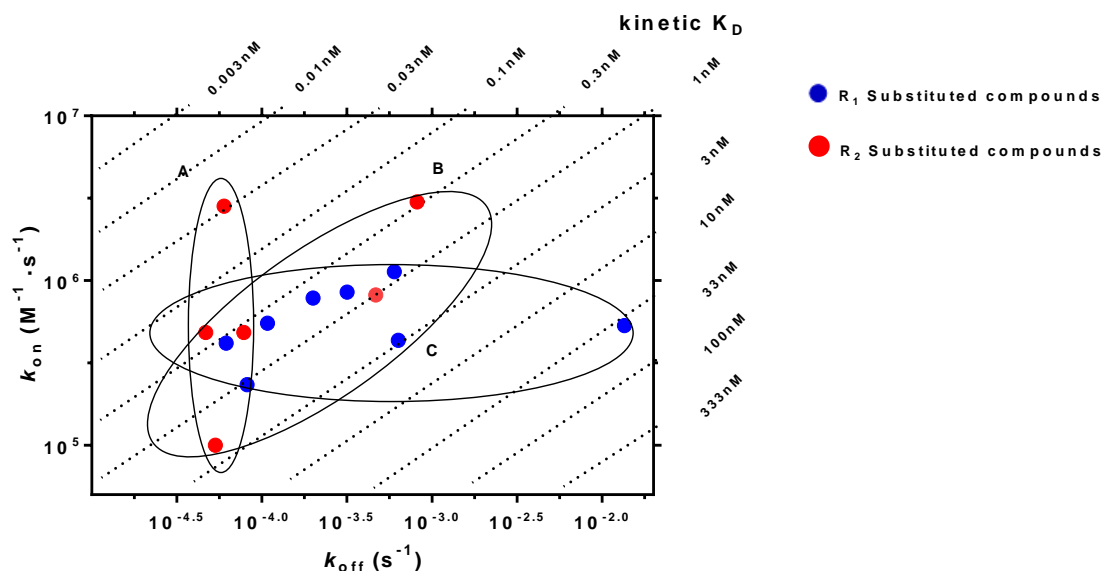
Figure 4: Kinetic map (y axis: k_{on} in $M^{-1} \cdot s^{-1}$, x axis: k_{off} in s^{-1}) of all compounds that were kinetically characterized in this study. k_{on} and k_{off} values were obtained through competition association assays performed at the hA$_3$R. The kinetically derived affinity (K$_D$ = k$_{off}$/k$_{on}$) is represented through diagonal parallel lines. Group A: compounds that show similar k$_{off}$ values but due to differing k$_{on}$ values have different K$_D$ values. Group B: compounds that display similar K$_D$ values despite showing divergent k$_{off}$ and k$_{on}$ values. Group C: compounds with similar k$_{on}$ values, but due to differing k$_{off}$ values have different K$_D$ values.

Altogether, the construction of a kinetic map allows for a more detailed categorization of compounds' affinities as dictated by their kinetic rate constants. In previous studies, such a separation has explained the different therapeutic effects molecules exhibit highlighting the benefits of such an in-depth analysis.[35, 36]

Given the putative link between RT and clinical efficacy, it may be postulated that the lack of hA$_3$R antagonists progressing from preclinical trials is due to insufficient selection criteria employed in these initial phases of hA$_3$R drug screening. As previously reported, hA$_3$R antagonists are reasoned to be beneficial in the treatment of Chronic Obstructive Pulmonary Disease (COPD).[37] For this indication, a number of antagonists are available that act at the muscarinic M$_3$ receptor.[38] For these therapeutics their dosing regime and thus duration of action have been linked to their RT. For example, aclidinium which requires a twice daily dosing regimen, exhibits a much shorter RT than tiotropium that in turn requires only once daily dosing.[16] This extended duration of action that

enables long-lasting efficacy and practical dosing regimens at the muscarinic M_3 receptor is thought to be a beneficial feature in the treatment of chronic illnesses.[39, 40] As hA_3R antagonists can be used to treat chronic COPD but also a number of other chronic disorders, we could imagine that considering the ligand's kinetic profile early in the drug screening process, would reduce the likelihood of failure due to insufficient efficacy in future clinical trials. Perhaps when selecting hA_3R antagonists with a favorable long RT, i.e. the group A in the kinetic map, will we see the therapeutic potential of the hA_3R fulfilled.

Computational studies.

Finally, we decided to further investigate the ligand-receptor interactions using a homology model of the adenosine A_3 receptor, based on the crystal structure of the adenosine A_{2A} receptor (PDB: 4EIY)[41]. WaterMap calculations were applied to try and explain the variance in kinetic profiles of different ligands by unfavorable hydration[42, 43].

Antagonist **2** (in black stick representation) was docked in the homology model. As a first step it was placed inside the transmembrane bundle, with the tricyclic ring system surrounded by TM3, TM6 and EL2. Hydrogen bonding was constrained between the amide-hydrogen (-NH_2, δ^+) from Asn250[6.55] and the carbonyl-oxygen (-C=O, δ^-) at the C^4-position of the pyrido[2,1-*f*]purine-2,4-dione scaffold (**Figure 5**, left). In order to compare differences between the ligands, an "apo" WaterMap of the hA_3 receptor was generated. Hydration sites shown as red and orange spheres represent positions where "unstable" water molecules are found. Antagonist **10** (hexyl-substitution), with comparable k_{off} ((8.2 ± 1.3) x 10^{-5} s^{-1} vs (6.0 ± 1.7) x 10^{-5} s^{-1}) to **2** but 10-fold slower k_{on} ((2.3 ± 1.0) x 10^5 $M^{-1}s^{-1}$ vs (2.8 ± 0.5) x 10^6 $M^{-1}s^{-1}$), was docked with two different binding modes in the same binding site (**Figure 5**, up-right, cyan and grey sticks). We found additional unstable waters (8, 11, 22 in **Figure 5**, up-right) surrounding the lipophilic substituents of the compounds, which could be explained as hindrance when the antagonist is associating with the binding site.
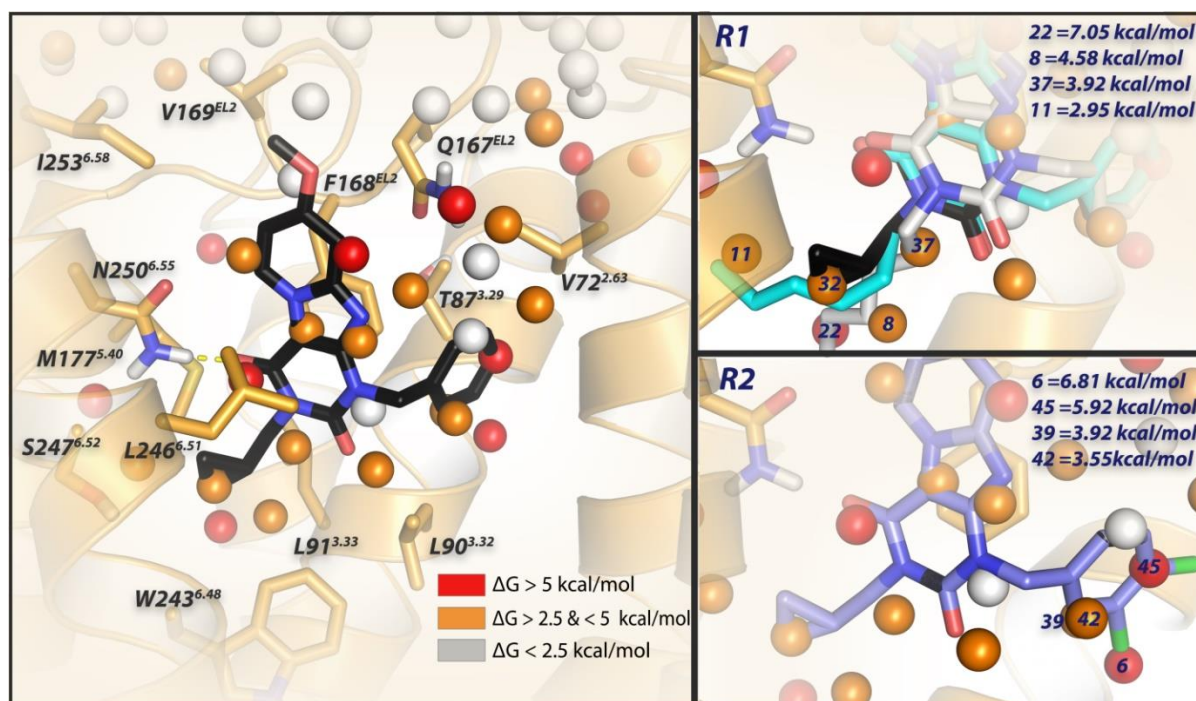
Figure 5. Docking of antagonist **2** into the binding site of the homology model of the adenosine A_3 receptor based on the crystal structure of the adenosine A_{2A} receptor (PDB: 4EIY).[41] Antagonist **2** is represented by black sticks, and residues within 5 Å of **2** are visualized as orange sticks. The protein is represented by orange ribbons. Ligand and residues atoms color code: red = oxygen, blue = nitrogen, white = hydrogen. The overlay of consecutively numbered hydration sites (colored spheres; for color code, see below) were calculated by WaterMap **(Left)**. Hydration sites shown as red and orange spheres represent positions were "unstable" water molecules can be found, which should be displaced by antagonist **2**. White spheres symbolize "stable" water molecules, which are in exchange with the bulk solvent. Two different binding modes are represented for antagonist **10** (cyan and grey sticks), which shows that the flexible hexyl chain can displace different hydration sites (8 for grey and 11 for cyan). For the key hydration sites (8, 11, 22, 32, 37) surrounding the lipophilic "tails", calculated ΔG values (in kcal/mol) with respect to bulk solvent are shown **(Up-right)**. Hydration sites 6, 39, 42 and 45 are proposed to be displaced by the 3,4 di-chloro substituents of **31**; calculated ΔG values (in kcal/mol) with respect to bulk solvent are shown **(Down-right)**.

The same WaterMap was used to investigate the kinetic profile of antagonist **31**. Indeed, hydration sites 6, 39, 42 and 45 are proposed to be displaced by the 3,4-dichloro substituent. Thus, both the association and dissociation of **31** were slowed down by these unstable waters. For the association process, the lipophilic 3,4-dichloro moiety has difficulty in approaching the occupied unstable hydration sites ($(1.0 \pm 0.1) \times 10^5$ M^{-1}s^{-1}, slowest k_{on} in the whole series); the same lipophilic 3,4-dichloro substituent seems to provide more stabilization to the receptor-ligand complex, thus hampering the dissociation process ($(5.3 \pm 1.5) \times 10^{-5}$ s^{-1}, slowest k_{off} in the whole series).

Interestingly, by removing a single chloro atom at either the 3- or 4- position on the benzyl-ring (**30** or **29**), association and dissociation rate constants became faster by approximately 10-fold. Although the differences in their k_{on} and k_{off} values were modest (2-3 fold), the unstable hydration sites may prevent the 4-chloro-substituted antagonist **30** from reaching the hydration sites 6, 39 and 42 that interact with the 3-Cl substituent; consequently, both its association and dissociation rate constants were faster than of the 3-chloro-substituted counterpart **29** (k_{on}: (3.0 ± 0.3) x 10^6 $M^{-1}s^{-1}$ vs (8.2 ± 1.3) x 10^5 $M^{-1}s^{-1}$; k_{off}: (8.2 ± 0.2) x 10^{-4} s^{-1} vs (4.7 ± 0.7) x 10^{-4} s^{-1}).

Conclusions

We have demonstrated that, next to affinity, additional knowledge of target binding kinetics is useful for selecting and developing new hA_3R antagonists in the early phase of drug discovery. By introducing proper substituents at the N^3 position or the N^1 benzyl ring of a series of pyridopurinediones, divergences in kinetic profiles were observed, while almost all compounds had high and often similar affinity. Two representative ligands (**5** and **27**) were tested in [^{35}S]GTPγS binding assays, confirming the link between their RTs and their (in)surmountable antagonism. According to these findings, a k_{on}-k_{off}-K_D kinetic map was constructed and subsequently the antagonists were divided into three sub-groups. Additionally, we also performed a computational modelling study that sheds light on the crucial interactions (including with water molecules) for both the association and dissociation kinetics of this family of antagonists. It should be mentioned that the kinetic parameters were derived at the hA_3R, which may be different in e.g., rodents used in advanced animal models. Still, this study suggests that favorable long RTs would be a proper indicator in the development of hA_3R antagonists for chronic inflammatory conditions, e.g. COPD.

Experimental section

Chemistry. All solvents and reagents were purchased from commercial sources and were of analytical grade. Distilled water will be referred to as H_2O. TLC analysis was performed to monitor

the reactions, using Merck silica gel F$_{254}$ plates. Grace Davison Davisil silica column material (LC60A, 30–200 μm) was used to perform column chromatography. Microwave reactions were performed in an Emrys Optimizer (Biotage AB, formerly Personal Chemistry). ^{1}H and ^{13}C NMR spectra were recorded on a Bruker DMX-400 (400 MHz) spectrometer, using tetramethylsilane as internal standard. Chemical shifts are reported in δ (ppm) and the following abbreviations are used: s, singlet; d, doublet; dd, double doublet; t, triplet; m, multiplet. The analytical purity of the final compounds is 95% or higher and was determined by high-performance liquid chromatography (HPLC) with a Phenomenex Gemini 3 μm C18 110A column (50 x 4.6 mm, 3 μm), measuring *UV* absorbance at 254 nm. The sample preparation and HPLC method was as follows: 0.3–0.6 mg of compound was dissolved in 1 mL of a 1:1:1 mixture of CH$_3$CN/H$_2$O/t-BuOH and eluted from the column within 15 min at a flow rate of 1.3 mL/min. The elution method was set up as follows: 1–4 min isocratic system of H$_2$O/CH$_3$CN/1% TFA in H$_2$O, 80:10:10; from the 4th min a gradient was applied from 80:10:10 to 0:90:10 within 9 min, followed by 1 min of equilibration at 0:90:10 and 1 min at 80:10:10. Liquid chromatography–mass spectrometry (LC–MS) analyses were performed using a Thermo Finnigan Surveyor—LCQ Advantage Max LC–MS system and a Gemini C18 Phenomenex column (50 x 4.6 mm, 3 μm). The elution method was set up as follows: 1–4 min isocratic system of H$_2$O/CH$_3$CN/1% TFA in H$_2$O, 80:10:10; from the 4th min a gradient was applied from 80:10:10 to 0:90:10 within 9 min, followed by 1 min of equilibration at 0:90:10 and 1 min at 80:10:10.

1-Benzyl-8-methoxy-1H,3H-pyrido[2,1-f]purine-2,4-dione (5.)[24] 6-Amino-1-benzyluracil (**4**) [25] (10.8 g, 49.7 mmol, 1.00 eq.) was suspended in CH$_3$CN (370 mL). *N*-bromosuccinimide (17.7 g, 99.4 mmol, 2.00 eq.) was added to the suspension and the mixture was heated at 80 ^{o}C for 1 hour, after which full conversion was shown by TLC (1:9 CH$_3$OH/CH$_2$Cl$_2$ + 3% triethylamine). Subsequently 4-methoxypyridine (15.1 mL, 149.2 mL, 3.00 eq.) was added and the mixture was heated at 80 ^{o}C during 10 hours. Full consumption of the bromo intermediate was shown by TLC (1% CH$_3$OH/CH$_2$Cl$_2$). A precipitate was formed overnight at RT which was collected by filtration and washed with diethyl

ether. This yielded the desired compound as a white solid (10.2 g, 31.6 mmol, 64%). ^{1}H NMR (400MHz, DMSO-d6) δ: 11.11 (s br, 1H), 8.72 (d, J = 7.2 Hz, 1H), 7.39-7.29 (m, 4H), 7.28-7.22 (m, 2H), 6.91 (dd, J = 7.2, 2.0 Hz, 1H), 5.19 (s, 2H), 3.89 (s, 3H) ppm. NMR was according to literature data.[24]

General procedure for the preparation of N[3]-substitited 1-benzyl-8-methoxy-1*H*,3*H*-pyrido[2,1-*f*]purine-2,4-diones (1, 2, 6-22).[24] The compounds were synthesized using the procedure described by *Priego et al.*,[24] but 5 eq. of the alkyl halide was used instead of 1.5 eq. and the reaction mixture was heated to 80 °C overnight in all cases. The pure compounds were obtained by silica column chromatography using a mixture of petroleum ether/ethyl acetate (2:1) as eluent, if not otherwise stated.

1-Benzyl-8-methoxy-3-propyl-1H,3H-pyrido[2,1-f]purine-2,4-dione (1).[24] The pure product was obtained by column chromatography using petroleum ether/ethyl acetate (1:1) as eluent, yielding a white solid 113 mg, 0.31 mmol, 60%. ^{1}H NMR (400MHz, CDCl₃) δ: 8.83 (d, J = 7.2 Hz, 1H), 7.54 (d, J = 7.2 Hz, 2H), 7.34-7.25 (m, 3H), 6.98 (d, J = 2.0 Hz, 1H), 6.74 (dd, J = 7.6, 2.8 Hz, 1H), 5.37 (s, 2H), 4.02 (t, J = 7.6 Hz, 2H), 3.92 (s, 3H), 1.74 (sextet, J = 7.6 Hz, 2H), 0.99 (t, J = 7.6 Hz, 3H) ppm.[24] MS [ESI+H]+: calcd for $C_{20}H_{20}N_4O_3$, 364.15; found, 365.0.

1-Benzyl-3-(cyclopropylmethyl)-8-methoxypyrido[2,1-f]purine-2,4(1H,3H)-dione (2).[23] The pure product was obtained by column chromatography using a mixture of 2% CH_3OH/CH_2Cl_2 as eluent, yielding a white solid, 1.51 g, 3.98 mmol, 86%. ^{1}H NMR (400MHz, CDCl₃) δ: 8.82 (d, J = 7.2 Hz, 1H), 7.54 (d, J = 7.2 Hz, 2H), 7.33-7.23 (m, 3H), 6.97 (d, J = 2.4 Hz, 1H), 6.73 (dd, J = 8.4, 2.4 Hz, 1H), 5.37 (s, 2H), 3.94 (d, J = 7.4 Hz, 2H), 3.92 (s, 3H), 1.35-1.25 (m, 1H), 0.47-0.44(m, 4H) ppm. MS [ESI+H]+: calcd for $C_{21}H_{20}N_4O_3$, 376.15; found, 376.9.

1-Benzyl-8-methoxy-3-methylpyrido[2,1-f]purine-2,4(1H,3H)-dione (6). Reaction was performed in a sealed tube and 50 eq. of methyl iodide was used. The residue was purified by silica column chromatography eluting with a petroleum ether/ethyl acetate (1:1) mixture, yielding a white solid,

25 mg, 0.074 mmol, 15%. ^{1}H NMR (400MHz, CDCl$_3$) δ: 8.83 (d, J = 7.6 Hz, 1H), 7.54 (d, J = 7.2 Hz, 2H), 7.33-7.24 (m, 3H), 6.99 (d, J = 2.4 Hz, 1H), 6.75 (dd, J = 7.6, 2.4 Hz, 1H), 5.37 (s, 2H), 3.93 (s, 3H), 3.45 (s, 3H) ppm. MS [ESI+H]$^+$: calcd for C$_{18}$H$_{16}$N$_4$O$_3$, 336.12; found, 337.2.

1-Benzyl-3-ethyl-8-methoxypyrido[2,1-f]purine-2,4(1H,3H)-dione (7). The pure product was obtained by column chromatography using petroleum ether/ethyl acetate (1:1) as eluent, yielding a white solid, 58 mg, 0.17 mmol, 33%. ^{1}H NMR (400MHz, CDCl$_3$) δ: 8.83 (d, J = 7.2 Hz, 1H), 7.54 (d, J = 7.2 Hz, 2H), 7.33-7.24 (m, 3H), 6.98 (d, J = 2.0 Hz, 1H), 6.74 (dd, J = 7.6, 2.8 Hz, 1H), 5.36 (s, 2H), 4.12 (q, J = 7.2 Hz, 2H), 3.92 (s, 3H), 1.28 (t, J = 7.2 Hz, 3H) ppm. MS [ESI+H]$^+$: calcd for C$_{19}$H$_{18}$N$_4$O$_3$, 350.14; found, 351.0.

1-Benzyl-3-butyl-8-methoxypyrido[2,1-f]purine-2,4(1H,3H)-dione (8). Purified by column chromatography using petroleum ether/EtOAc (3:1), yielding a white solid 10 mg, 0.026 mmol, 5%. ^{1}H NMR (400MHz, CDCl$_3$) δ: 8.83 (d, J = 7.6 Hz, 1H), 7.54 (d, J = 6.8 Hz, 2H), 7.24-7.33 (m, 3H), 6.98 (d, J = 2.4 Hz, 1H), 6.74 (dd, J = 7.4, 2.6 Hz, 1H), 5.36 (s, 2H), 4.04 (t, J = 7.6 Hz, 2H), 3.93 (s, 3H), 1.70-1.64 (m, 2H), 1.40 (sextet, J = 3.6 Hz, 2H), 0.95 (t, J = 7.2 Hz, 3H) ppm. MS [ESI+H]$^+$: calcd for C$_{21}$H$_{22}$N$_4$O$_3$, 378.17; found, 378.9.

1-Benzyl-8-methoxy-3-pentyl-1H,3H-pyrido[2,1-f]purine-2,4-dione (9). White solid, 110 mg, 0.28 mmol, yield 56%. ^{1}H NMR (400MHz, CDCl$_3$) δ: 8.83 (d, J = 7.6 Hz, 1H), 7.56 (d, J = 7.2 Hz, 2H), 7.34-7.25 (m, 3H), 6.97 (d, J = 2.0 Hz, 1H), 6.74 (dd, J = 7.6, 2.8 Hz, 1H), 5.37 (s, 2H), 4.05 (t, J = 7.6 Hz, 2H), 3.93 (s, 3H), 1.72-1.66 (m, 2H), 1.39-1.37 (m, 4H), 0.91 (t, J = 7.2 Hz, 3H) ppm. MS [ESI+H]$^+$: calcd for C$_{22}$H$_{24}$N$_4$O$_3$, 392.18; found, 393.1.

1-Benzyl-3-hexyl-8-methoxypyrido[2,1-f]purine-2,4(1H,3H)-dione (10). White solid, 90 mg, 0.22 mmol, yield 44%. ^{1}H NMR (400MHz, CDCl$_3$) δ: 8.83 (d, J = 7.2 Hz, 1H), 7.55 (d, J = 6.8 Hz, 2H), 7.34-7.25 (m, 3H), 6.98 (d, J = 2.0 Hz, 1H), 6.74 (dd, J = 7.6, 2.4 Hz, 1H), 5.37 (s, 2H), 4.05 (t, J = 7.6 Hz, 2H),

3.92 (s, 3H), 1.69 (pentet, *J* = 7.6 Hz, 2H), 1.40-1.26 (m, 6H), 0.89 (t, *J* = 7.2 Hz, 3H) ppm. MS [ESI+H]$^+$: calcd for C$_{23}$H$_{26}$N$_4$O$_3$, 406.20; found, 407.1.

1-Benzyl-3-heptyl-8-methoxypyrido[2,1-f]purine-2,4(1H,3H)-dione **(11)**. Column chromatography using a mixture of petroleum ether/ethyl acetate (3:1) as eluent yielded 131 mg of the pure product as white solid, 0.31 mmol, 62%. 1H NMR (400MHz, CDCl$_3$) ^{1}H NMR (400MHz, CDCl3) δ: 8.80 (d, *J* = 7.6 Hz, 1H), 7.54 (d, *J* = 6.8 Hz, 2H), 7.32-7.25 (m, 3H), 6.95 (d, *J* = 2.4 Hz, 1H), 6.71 (dd, *J* = 7.2, 2.4 Hz, 1H), 5.35 (s, 2H), 4.03 (t, *J* = 7.6, 2H), 3.90 (s, 3H), 1.67 (pentet, *J* = 7.6 Hz, 2H), 1.38-1.26 (m, 8H), 0.87 (t, *J* = 7.2 Hz, 3H) ppm. MS [ESI+H]$^+$: calcd for C$_{24}$H$_{48}$N$_4$O$_3$, 420.22; found, 421.2.

3-Allyl-1-benzyl-8-methoxypyrido[2,1-f]purine-2,4(1H,3H)-dione **(12)**. Purified by column chromatography using petroleum ether/ethyl acetate (1:1) as eluent, yielding a white solid, 73 mg, 0.20 mmol, 40%. ^{1}H NMR (400MHz, CDCl$_3$) δ: 8.82 (d, *J* = 7.6 Hz, 1H), 7.55 (d, *J* = 7.2 Hz, 2H), 7.34-7.25 (m, 3H), 6.99 (d, *J* = 2.0 Hz, 1H), 6.75 (dd, *J* = 7.6, 2.4 Hz, 1H), 6.02-5.92 (m, 1H), 5.38 (s, 2H), 5.29 (dd, *J* = 17.2, 1.2 Hz, 1H), 5.20 (d, *J* = 10.0 Hz, 1H), 4.68 (d, *J* = 5.6 Hz, 2H), 3.93 (s, 3H) ppm. MS [ESI+H]$^+$: calcd for C$_{20}$H$_{18}$N$_4$O$_3$, 362.14; found, 363.0.

1-Benzyl-8-methoxy-3-(prop-2-yn-1-yl)pyrido[2,1-f]purine-2,4(1H,3H)-dione **(13)**. The pure product was obtained by column chromatography using petroleum ether/ethyl acetate (1:1) as eluent, yielding a white solid, 60 mg, 0.17 mmol, 3%. ^{1}H NMR (400MHz, CDCl$_3$) δ: 8.82 (d, *J* = 7.2 Hz, 1H), 7.57 (d, *J* = 6.8 Hz, 2H), 7.36-7.26 (m, 3H), 6.99 (d, *J* = 2.4 Hz, 1H), 6.76 (dd, *J* = 7.2, 2.4 Hz, 1H), 5.38 (s, 2H), 4.83 (d, *J* = 2.4 Hz, 2H), 3.94 (s, 3H), 2.19 (t, *J* = 2.4 Hz, 1H) ppm. MS [ESI+H]$^+$: calcd for C$_{20}$H$_{16}$N$_4$O$_3$, 360.12; found, 361.1.

1-Benzyl-3-(but-3-en-1-yl)-8-methoxypyrido[2,1-f]purine-2,4(1H,3H)-dione **(14)**. White solid, 18 mg, 0.05 mmol, yield 10%. ^{1}H NMR (400MHz, CDCl$_3$) δ: 8.84 (d, *J* = 7.6 Hz, 1H), 7.54 (d, *J* = 7.2 Hz, 2H), 7.35-7.28 (m, 3H), 7.00 (d, *J* = 2.4 Hz, 1H), 6.77 (dd, *J* = 7.6, 2.4 Hz, 1H), 5.91-5.84 (m, 1H), 5.39 (s,

2H), 5.08 (dd, J = 16.8, 1.2 Hz, 1H), 5.02 (d, J = 10.4, 1H), 4.15 (t, J = 7.2 Hz, 2H), 3.95 (s, 3H), 2.48 (q, J = 7.2 Hz, 2H) ppm. MS [ESI+H]$^+$: calcd for $C_{21}H_{20}N_4O_3$, 376.15; found, 376.9.

1-Benzyl-8-methoxy-3-(2-methoxyethyl)-1H,3H-pyrido[2,1-f]purine-2,4-dione (**15**). Purified by column chromatography using a mixture of 2% CH_3OH in CH_2Cl_2 yielded the product as a white solid, 70 mg, 0.18 mmol, 37%. ^{1}H NMR (400MHz, CDCl$_3$) δ: 8.83 (d, J = 7.2 Hz, 1H), 7.54 (d, J = 6.8 Hz, 2H), 7.33-7.24 (m, 3H), 6.98 (d, J = 2.4 Hz, 1H), 6.74 (dd, J = 7.6, 2.4 Hz, 1H), 5.36 (s, 2H), 4.30 (t, J = 6.0 Hz, 2H), 3.93 (s, 3H), 3.68 (t, J = 6.0 Hz, 2H), 3.36 (s, 3H) ppm. MS [ESI+H]$^+$: calcd for $C_{20}H_{20}N_4O_3$, 380.15; found, 380.8.

1-Benzyl-3-(3-hydroxypropyl)-8-methoxypyrido[2,1-f]purine-2,4(1H,3H)-dione (**16**). Purified by column chromatography using a mixture of petroleum ether/EtOAc (1:2), followed by recrystallization from CH_3OH/EtOAc. Yield: white solid, 106 mg, 0.28 mmol, 28%. ^{1}H NMR (400MHz, CDCl$_3$) δ: 8.80 (d, J = 7.2 Hz, 1H), 7.53 (d, J = 7.6 Hz, 2H), 7.33-7.24 (m, 3H), 6.99 (d, J = 2.4 Hz, 1H), 6.76 (dd, J = 7.6, 2.4 Hz, 1H), 5.37 (s, 2H), 4.22 (t, J = 6.0 Hz, 2H), 3.93 (s, 3H), 3.53 (t, J = 5.6 Hz, 2H), 1.92 (pentet, J = 5.6 Hz, 2H) ppm. MS [ESI+H]$^+$: calcd for $C_{20}H_{20}N_4O_3$, 380.15; found, 380.9.

1-Benzyl-3-isobutyl-8-methoxypyrido[2,1-f]purine-2,4(1H,3H)-dione (**17**). White solid, 0.08 mmol, 29 mg, yield 15%. ^{1}H NMR (400MHz, CDCl$_3$) δ: 8.86 (d, J = 7.2 Hz, 1H), 7.55 (d, J = 7.2 Hz, 2H), 7.33-7.28 (m, 3H), 7.00 (d, J = 2.0 Hz, 1H), 6.76 (dd, J = 7.6, 2.4 Hz, 1H), 5.39 (s, 2H), 3.95 (s, 3H), 3.92 (d, J = 7.6 Hz, 2H), 2.22 (nonet, J = 7.2 Hz, 1H), 0.97 (d, J = 6.8 Hz, 6H) ppm. MS [ESI+H]$^+$: calcd for $C_{21}H_{22}N_4O_3$, 378.17; found, 379.0.

1-Benzyl-8-methoxy-3-(3-neopentyl)-1H,3H-pyrido[2,1-f]purine-2,4-dione (**18**). Purified by column chromatography using a mixture of 1% CH_3OH in CH_2Cl_2 as eluent, yielding the product as a white solid, 0.025 mmol, 20mg, 5%. ^{1}H NMR (400MHz, CDCl$_3$) δ: 8.84 (d, J = 7.2 Hz, 1H), 7.52 (d, J = 7.2 Hz, 2H), 7.32-7.25 (m, 3H), 6.98 (d, J = 2.4 Hz, 1H), 6.73 (dd, J = 7.2, 2.4 Hz, 1H), 5.37 (s, 2H), 3.99 (s, 2H), 3.92 (s, 3H), 0.98 (s, 9H) ppm. MS [ESI+H]$^+$: calcd for $C_{22}H_{24}N_4O_3$, 392.18; found, 393.0.

1-Benzyl-3-isopentyl-8-methoxypyrido[2,1-f]purine-2,4(1H,3H)-dione (19). Yield: white solid, 104 mg, 0.26 mmol, 53%. ^{1}H NMR (400MHz, CDCl$_3$) δ: 8.83 (d, *J* = 7.2 Hz, 1H), 7.53 (d, *J* = 7.2 Hz, 2H), 7.33-7.24 (m, 3H), 6.98 (d, *J* = 2.4 Hz, 1H), 6.74 (dd, *J* = 7.6, 2.4 Hz, 1H), 5.36 (s, 2H), 4.08-4.04 (m, 2H), 3.93 (s, 3H), 1.69 (nonet, *J* = 6.8 Hz, 1H), 1.59-1.53 (m, 2H), 0.98 (d, *J* = 6.4 Hz, 6H) ppm. MS [ESI+H]$^+$: calcd for C$_{22}$H$_{24}$N$_4$O$_3$, 392.18; found, 393.1.

1-Benzyl-3-(3,3-dimethylbutyl)-8-methoxy-pyrido[2,1-f]purine-2,4(1H,3H)-dione (20). Yield: white solid, 81 mg, 0.20 mmol, 40%. [1]NMR (400MHz, CDCl$_3$) δ: 8.84 (d, *J* = 7.6 Hz, 1H), 7.55 (d, *J* = 7.2, 2H), 7.35-7.27 (m, 3H), 6.98 (d, *J* = 2.4 Hz, 1H), 6.74 (dd, *J* = 7.2, 2.4 Hz, 1H), 5.38 (s, 2H), 4.12-4.08 (m, 2H), 3.93 (s, 3H), 1.61-1.57 (m, 2H), 1.04 (s, 9H) ppm. MS [ESI+H]$^+$: calcd for C$_{23}$H$_{26}$N$_4$O$_3$, 406.20; found, 407.1.

1-Benzyl-8-methoxy-3-((trimethylsilyl)methyl)pyrido[2,1-f]purine-2,4(1H,3H)-dione (21). White solid, 137 mg, 0.34 mmol, yield 67%. ^{1}H NMR (400MHz, CDCl$_3$) δ: 8.84 (d, *J* = 7.2 Hz, 1H), 7.50 (d, *J* = 6.8 Hz, 2H), 7.32-7.24 (m, 3H), 6.98 (d, *J* = 2.4 Hz, 1H), 6.73 (d, *J* = 7.2, 2.4 Hz, 1H), 5.39 (s, 2H), 3.93 (s, 3H), 3.64 (s, 2H), 0.08 (s, 9H) ppm. MS [ESI+H]$^+$: calcd for C$_{21}$H$_{24}$N$_4$O$_3$Si, 408.16; found, 409.2.

1-Benzyl-3-(cyclobutylmethyl)-8-methoxypyrido[2,1-f]purine-2,4(1H,3H)-dione (22). White solid, 90 mg, 0.23 mmol, yield 46%. ^{1}H NMR (400MHz, CDCl$_3$) δ: 8.82 (d, *J* = 7.2 Hz, 1H), 7.53 (d, *J* = 7.2 Hz, 2H), 7.33-7.13 (m, 3H), 6.69 (d, *J* = 1.8 Hz, 1H), 6.73 (dd, *J* = 7.2, 2.4 Hz, 1H), 5.35 (s, 2H), 4.11 (d, *J* = 7.6 Hz, 2H), 3.92 (s, 3H), 2.83-2.72 (m, 1H), 2.05-1.95 (m, 2H), 1.90-1.79 (m, 4H) ppm. MS [ESI+H]$^+$: calcd for C$_{22}$H$_{22}$N$_4$O$_3$, 390.17; found, 391.2.

3-(Cyclopropylmethyl)-8-methoxypyrido[2,1-f]purine-2,4(1H,3H)-dione (23).[23] Prepared following a slightly modified procedure described by Priego et al. In total 4 portions of 8 eq. of ammonium formate (after 0, 2, 4 and 6 hours) and 3 portions of 0.15 eq. of 20% Pd(OH)$_2$ (0, 4 and 6 hours) were added, after which full conversion was reached after overnight reflux visualized by TLC (3% CH$_3$OH/CH$_2$Cl$_2$). The reaction mixture was filtered over Celite and the residue extracted 5 times with

hot DMF. The combined organic layer was concentrated *in vacuo* which resulted in a quantitative yield. ^{1}H-NMR in accordance to data in literature.[23]

General procedure for the preparation of N[1]-substitited-3-cyclopropylmethyl-8-methoxy-1*H*,3*H*-pyrido[2,1-*f*]purine-2,4-diones (24-33).[23] The compounds were synthesized according to the procedure described by *Priego et al.*[2] Purification by silica column chromatography using an eluent mixture of petroleum ether/ethyl acetate (3:1) yielded the pure final products.

3-(Cyclopropylmethyl)-8-methoxy-1-(3-methylbenzyl)pyrido[2,1-f]purine-2,4(1H,3H)-dione **(24)**. White solid, 79 mg, 0.20 mmol, yield 57%. ^{1}H NMR (400MHz, CDCl$_3$) δ: 8.84 (d, *J* = 7.2 Hz, 1H), 7.36 (s, 2H), 7.22 (t, *J* = 7.6 Hz, 1H), 7.09 (d, *J* = 7.6 Hz, 1H), 6.99 (d, *J* = 2.4 Hz, 1H), 6.75 (dd, *J* = 7.2, 2.4 Hz, 1H), 5.36 (s, 2H), 3.97 (d, *J* = 7.2 Hz, 2H), 3.94 (s, 3H), 2.34 (s, 3H), 1.37-1.31 (m, 1H), 0.52-0.45 (m, 4H) ppm. MS [ESI+H]$^+$: calcd for C$_{22}$H$_{22}$N$_4$O$_3$, 390.17; found, 391.0.

3-(Cyclopropylmethyl)-8-methoxy-1-(4-methylbenzyl)pyrido[2,1-f]purine-2,4(1H,3H)-dione **(25)**.[23]

3-(Cyclopropylmethyl)-1-(4-ethylbenzyl)-8-methoxypyrido[2,1-f]purine-2,4(1H,3H)-dione **(26)**. White solid, 43 mg, 0.11 mmol, yield 21%. ^{1}H NMR (400MHz, CDCl$_3$) δ: 8.82 (d, *J* = 7.6 Hz, 1H), 7.48 (d, *J* = 8.0 Hz, 2H), 7.14 (d, *J* = 8.0 Hz, 2H), 6.98 (d, *J* = 2.0 Hz, 1H), 6.73 (dd, *J* = 7.2, 2.4 Hz, 1H), 5.34 (s, 2H), 3.95-3.93 (m, 5H), 2.60 (q, *J* = 7.6 Hz, 2H), 1.34-1.28 (m, 1H), 1.19 (t, *J* = 7.6 Hz, 3H), 0.50-0.42 (m, 4H) ppm. MS [ESI+H]$^+$: calcd for C$_{23}$H$_{24}$N$_4$O$_3$, 404.18; found, 405.2.

3-(Cyclopropylmethyl) -8-methoxy-1-(3-methoxybenzyl)pyrido[2,1-f]purine-2,4(1H,3H)-dione **(27)**. White solid, 20 mg, 0.049 mmol, yield 14%. ^{1}H NMR (400MHz, CDCl$_3$) δ: 8.83 (d, *J* = 7.6 Hz, 1H), 7.23 (t, *J* = 8.0 Hz, 1H), 7.15-7.10 (m, 2H), 6.97 (d, *J* = 1.6 Hz, 1H), 6.80 (dd, *J* = 8.4, 2.4 Hz, 1H), 6.74 (dd, *J* = 7.6, 2.4 Hz, 1H), 5.35 (s, 2H), 3.96-3.92 (m, 5H), 3.77 (s, 3H), 1.35-1.28 (m, 1H), 0.50-0.45 (m, 4H) ppm. MS [ESI+H]$^+$: calcd for C$_{22}$H$_{22}$N$_4$O$_4$, 406.16; found, 406.9.

3-(Cyclopropylmethyl)-8-methoxy-1-(4-methoxybenzyl)pyrido[2,1-f]purine-2,4(1H,3H)-dione **(28)**.[23]

148

1-(3-Chlorobenzyl)-3-(cyclopropylmethyl)-8-methoxypyrido[2,1-f]purine-2,4(1H,3H)-dione **(29)**.[23]

1-(4-Chlorobenzyl)-3-(cyclopropylmethyl)-8-methoxypyrido[2,1-f]purine-2,4(1H,3H)-dione **(30)**.[23]

3-(Cyclopropylmethyl)-1-(3,4-dichlorobenzyl)-8-methoxypyrido[2,1-f]purine-2,4(1H,3H)-dione **(31)**.[23]

1-(4-Bromobenzyl)-3-(cyclopropylmethyl)-8-methoxypyrido[2,1-f]purine-2,4(1H,3H)-dione **(32)**. White solid, 22 mg, 0.048 mmol, yield 14%. ^{1}H NMR (400MHz, CDCl$_3$) δ: 8.85 (d, *J* = 7.2 Hz, 1H), 7.46 (s, 4H), 6.99 (d, *J* = 1.6 Hz, 1H), 6.87 (dd, *J* = 7.2, 2.0 Hz, 1H), 5.33 (s, 2H), 3.99-3.85 (m, 5H), 1.34-1.24 (m, 1H), 0.50-0.44 (m, 4H) ppm. MS [ESI+H]$^+$: calcd for C$_{21}$H$_{19}$N$_4$O$_3$, 454.06; found, 455.0.

3-(Cyclopropylmethyl) -8-methoxy-1-phenylethylpyrido[2,1-f]purine-2,4(1H,3H)-dione **(33)**. White solid, 112 mg, 0.29 mmol, yield 82%. ^{1}H NMR (400MHz, CDCl$_3$) δ: 8.81 (d, *J* = 7.2 Hz, 1H), 7.35-7.25 (m, 4H), 7.20 (t, *J* = 7.2 Hz, 1H), 6.96 (d, *J* = 2.4 Hz, 1H), 6.73 (dd, *J* = 7.2, 2.4 Hz, 1H), 4.40 (t, *J* = 8.0 Hz, 2H), 3.95-3.90 (m, 5H), 3.12 (t, *J* = 8.0 Hz, 2H), 1.32-1.23 (m, 1H), 0.49-0.40 (m, 4H) ppm. MS [ESI+H]$^+$: calcd for C$_{22}$H$_{22}$N$_4$O$_3$, 390.17; found, 391.0.

Biology. *Chemicals and Reagents.* [^{3}H]8-Ethyl-4-methyl-2-phenyl-(8*R*)-4,5,7,8-tetrahydro-1*H*-imidazo[2,1-*i*]-purin-5-one[26] ([^{3}H]**34**, specific activity 56 Ci·mmol^{-1}) was a gift from Prof. C.E. Müller (University of Bonn, Germany). Unlabeled **34** was purchased from Tocris Ltd. (Abingdon, UK). 5'-*N*-ethylcarboxamidoadenosine (NECA) was purchased from Sigma-Aldrich (Steinheim, Germany). Adenosine deaminase (ADA) was purchased from Boehringer Mannheim (Mannheim, Germany). Bicinchoninic acid (BCA) and BCA protein assay reagents were purchased from Pierce Chemical Company (Rockford, IL, USA). Chinese hamster ovary cells stably expressing the human adenosine A$_3$ receptor (CHOhA$_3$) were a gift from Dr. K-N Klotz (University of Würzburg, Germany). All other chemicals were obtained from standard commercial sources and were of analytical grade.

Cell Culture and Membrane Preparation. Chinese Hamster Ovary (CHO) cells, stably expressing the human adenosine A$_3$ receptor (CHOhA$_3$), were cultured and membranes were prepared and stored

as previously described[44]. Protein determination was done through use of the bicinchoninic acid (BCA) method[45].

Radioligand Displacement Assay. Membrane aliquots containing ~15 μg of CHOhA$_3$ protein were incubated in a total volume of 100 μL assay buffer (50 mM Tris-HCl, 5 mM MgCl$_2$, supplemented with 0.01% CHAPS and 1 mM EDTA, pH 7.4) at 25 °C for 120 min. Displacement experiments were performed using 6 concentrations of competing antagonist in the presence of a final concentration of ~10 nM [^{3}H] **34**. At this concentration, total radioligand binding did not exceed 10% of that added to prevent ligand depletion. Nonspecific binding (NSB) was determined in the presence of 100 μM NECA. Incubation was terminated by rapid filtration performed on 96-well GF/B filter plates (Perkin Elmer, Groningen, the Netherlands), using a PerkinElmer Filtermate-harvester (Perkin Elmer, Groningen, the Netherlands). After drying the filter plate at 50 °C for 30 min, the filter-bound radioactivity was determined by scintillation spectrometry using the 2450 MicroBeta^2 Plate Counter (Perkin Elmer, Boston, MA).

Radioligand association and dissociation assays. Association experiments were performed by incubating membrane aliquots containing ~15 μg of CHOhA$_3$ membrane in a total volume of 100 μL of assay buffer at 10 or 25 °C with ~10 nM [^{3}H] **34**. The amount of radioligand bound to the receptor was measured at different time intervals during a total incubation of 120 min. Dissociation experiments were performed by preincubating membrane aliquots containing ~15 μg of protein in a total volume of 100 μL of assay buffer at 10 or 25 °C for 60 min. After the preincubation, radioligand dissociation was initiated by the addition of 5 μl 100 μM unlabeled NECA. The amount of radioligand still bound to the receptor was measured at various time intervals for a total of 120 min to ensure that full dissociation from hA$_3$ receptor was reached. Incubations were terminated and samples were obtained as described under *Radioligand Displacement Assay*.

Radioligand Competition Association Assay. The binding kinetics of unlabeled ligands were quantified using the competition association assay based on the theoretical framework by Motulsky

150

and Mahan.[46] The competition association assay was initiated by adding membrane aliquots (15 µg/well) at different time points for a total of 240 min to a total volume of 100 µl of assay buffer at 10 °C or 25 °C with ~10 nM [^{3}H] **34** in the absence or presence of a single concentration of competing hA$_3$R antagonists (i.e. at their IC$_{50}$ value). Incubations were terminated and samples were obtained as described under *Radioligand Displacement Assay*. The "dual-point" competition association assays were designed as described previously,[27] where in this case the two time points were selected at 20 (t$_1$) and 240 min (t$_2$).

[^{35}S] GTPγS Binding Assay. The assays were performed by incubating 15 µg of homogenized CHOhA$_3$ membranes in a total volume of 80 µl assay buffer (50 mM Tris-HCl buffer, 5 mM MgCl$_2$, 1 mM EDTA, 0.05% BSA and 1 mM DTT, pH 7.4) supplemented with 1 µM GDP and 5 µg saponin. The assays were performed in a 96-well plate format, where DMSO stock solutions of the compounds were added using a HP D300 Digital Dispenser (Tecan, Männedorf, Switserland). The final concentration of organic solvent per assay point was ≤0.1%. In all cases, the basal level of [^{35}S] GTPγS binding was measured in untreated membrane samples, whereas the maximal level of [^{35}S] GTPγS binding was measured by treatment of the membranes with 10 µM 2-Cl-IBMECA. For the insurmountability experiments, membrane preparations were pre-incubated with or without antagonists (30-, 100-, 300-fold Ki values) for 60 min at 25 °C, prior to the addition of 2-Cl-IBMECA (10 µM to 0.1 nM) and 20 µl [^{35}S] GTPγS (final concentration ~0.3 nM), after which incubation continued for another 30 min at 25 °C. For the surmountability (control) experiments, antagonists and 2-Cl-IBMECA were co-incubated with [^{35}S] GTPγS for 30 min at 25 °C. For all experiments, incubations were terminated and samples were obtained as described under *Radioligand Displacement Assay*, by using GF/B filters (Whatman International, Maidstone, UK).

Data Analysis. All experimental data were analyzed using the nonlinear regression curve fitting program GraphPad Prism 6.0 (GraphPad Software, Inc., San Diego, CA). From displacement assays, IC$_{50}$ values were obtained by non-linear regression analysis of the displacement curves. The obtained

IC$_{50}$ values were converted into K$_i$ values using the Cheng-Prusoff equation to determine the affinity of the ligands.[47] The observed association rates (k$_{obs}$) derived from both assays were obtained by fitting association data using one phase exponential association. The dissociation rates were obtained by fitting dissociation data to a one phase exponential decay model. The k$_{obs}$ values were converted into association rate constants (k$_{on}$) using the equation k$_{on}$ = (k$_{obs}$ − k$_{off}$)/[L], where [L] is the amount of radioligand used for the association experiments. The association and dissociation rates were used to calculate the kinetic K$_D$ using the equation K$_D$ = k$_{off}$/k$_{on}$. Association and dissociation rate constants for unlabeled compounds were calculated by fitting the data into the competition association model using "kinetics of competitive binding":[46]

$$K_A = k_1[L] \cdot 10^{-9} + k_2$$
$$K_B = k_3[I] \cdot 10^{-9} + k_4$$
$$S = \sqrt{(K_A - K_B)^2 + 4 \cdot k_1 \cdot k_3 \cdot L \cdot I \cdot 10^{-18}}$$
$$K_F = 0.5(K_A + K_B + S)$$
$$K_S = 0.5(K_A + K_B - S)$$
$$Q = \frac{B_{max} \cdot k_1 \cdot L \cdot 10^{-9}}{K_F - K_S}$$
$$Y = Q \cdot \left(\frac{k_4 \cdot (K_F - K_S)}{K_F \cdot K_S} + \frac{k_4 - K_F}{K_F} e^{(-K_F \cdot X)} - \frac{k_4 - K_S}{K_S} e^{(-K_S \cdot X)} \right)$$

where k$_1$ is the k$_{on}$ of the radioligand (M^{-1}s^{-1}), k$_2$ is the k$_{off}$ of the radioligand (s^{-1}), L is the radioligand concentration (nM), I is the concentration of the unlabeled competitor (nM), X is the time (s) and Y is the specific binding of the radioligand (DPM). The control curve (without competitor) from competition association assays generates the k$_1$ value and the k$_2$ value was obtained from *Radioligand association and dissociation assays*. With that the k$_3$, k$_4$ and B$_{max}$ can be calculated, where k$_3$ represents the k$_{on}$ (M^{-1}s^{-1}) of the unlabeled ligand, k$_4$ stands for the k$_{off}$ (s^{-1})of the unlabeled ligand and B$_{max}$ equals the total binding (DPM). All competition association data were globally fitted. The residence time (RT, in min) was calculated using the equation RT = 1/(60*k$_{off}$), as k$_{off}$ values are expressed in s^{-1}. [^{35}S] GTPγS binding curves were analyzed by nonlinear regression using "log

(agonist) vs response-variable slope" to obtain potency, inhibitory potency or efficacy values of agonists and inverse agonists/antagonists (EC_{50}, IC_{50} or E_{max}, respectively). In the (in)surmountability assays, Gaddum/Schild EC_{50} shift equations were used to obtain Schild-slopes and pA_2 values; statistical analysis of two-way ANOVA with Tukey's post-test was applied. All experimental values obtained are means of at least three independent experiments performed in duplicate, unless stated otherwise. R^2 and P values were calculated using the GraphPad Prism linear regression analysis function. Log$P$ (log partition coefficient) values were calculated using Chemdraw Professional 15.0 (Cambridge Soft, Perkin Elmer, Waltham Mass).

Computational studies. A ligand optimized homology model of the hA_3R was generated, following a similar approach as has been used before[48] and using the Maestro software package (Schroedinger Inc, New York). In short: first different homology models were constructed based on the high resolution crystal structure of the adenosine A_{2A} receptor (PDB: 4EIY),[41] and using a sequence alignment from GPCRDB.[49, 50] In the subsequent steps we iteratively optimized the model using Prime.[51-53] During every step the best model was selected based on enrichment (BEDROC-160.9 and ROC). For this we used a set of 100 diverse antagonists from ChEMBL[54] obtained by "Cluster Molecules".[55] We matched 50 decoys to every ligand ionization state, using the DUD-e web service.[56] The final model used here showed excellent enrichment (BEDROC-160.9: 0.55 ROC: 0.80). We introduced a long residence time ligand, **2**, in the putative ligand binding site using Induced fit docking,[57] with H-bond constraints on Asn250[6.55]. Based on this we generated a WaterMap[42, 43] of the apo state of the receptor. Other ligands were docked using core-constrained docking (using the core of **2** as constraints). Figures were rendered using PyMol.[58]

References

1.   Meyerhof, W.; Müller-Brechlin, R.; Richter, D. Molecular cloning of a novel putative G-protein coupled receptor expressed during rat spermiogenesis. *FEBS Lett.* **1991,** 284, 155-160.

2.   Fredholm, B. B.; IJzerman, A. P.; Jacobson, K. A.; Klotz, K.-N.; Linden, J. International union of pharmacology. XXV. nomenclature and classification of adenosine receptors. *Pharmacol. Rev.* **2001,** 53, 527-552.

3.   Jacobson, K. A.; Gao, Z.-G. Adenosine receptors as therapeutic targets. *Nat. Rev. Drug Discov.* **2006,** 5, 247-264.

4.   Gessi, S.; Merighi, S.; Varani, K.; Leung, E.; Mac Lennan, S.; Borea, P. A. The A3 adenosine receptor: an enigmatic player in cell biology. *Pharmacol. Ther.* **2008,** 117, 123-140.

5.   Jacobson, K. A.; Moro, S.; Kim, Y.-C.; Li, A.-H. A3 adenosine receptors: protective vs. damaging effects identified using novel agonists and antagonists. *Drug Dev. Res.* **1998,** 45, 113-124.

6.   Shamama, N.; Luqman, A. K.; Zafar, M. A.; Seemi, F. B. Adenosine A3 receptor: a promising therapeutic target in cardiovascular disease. *Curr. Cardiol. Rev.* **2016,** 12, 18-26.

7.   Koscsó, B.; Csóka, B.; Pacher, P.; Haskó, G. Investigational A3 adenosine receptor targeting agents. *Expert Opin. Invest. Drugs* **2011,** 20, 757-768.

8.   Fishman, P.; Bar-Yehuda, S.; Synowitz, M.; Powell, J. D.; Klotz, K. N.; Gessi, S.; Borea, P. A. Adenosine receptors and cancer. *Handb. Exp. Pharmacol.* **2009**, 399-441.

9.   Zhou, Y.; Schneider, D. J.; Blackburn, M. R. Adenosine signaling and the regulation of chronic lung disease. *Pharmacol. Ther.* **2009,** 123, 105-116.

10.   Wilson, C. N.; Nadeem, A.; Spina, D.; Brown, R.; Page, C. P.; Jamal Mustafa, S. Adenosine receptors and asthma. *Handb. Exp. Pharmacol.* **2009**, 10.1007/1978-1003-1540-89615-89619_89611.

11.   Wilson, C. N. Adenosine receptors and asthma in humans. *Br. J. Pharmacol.* **2008,** 155, 475-486.

12.   Borea, P. A.; Varani, K.; Vincenzi, F.; Baraldi, P. G.; Tabrizi, M. A.; Merighi, S.; Gessi, S. The A3 adenosine receptor: history and perspectives. *Pharmacol. Rev.* **2015,** 67, 74-102.

13.   Baraldi, P. G.; Cacciari, B.; Romagnoli, R.; Merighi, S.; Varani, K.; Borea, P. A.; Spalluto, G. A3 adenosine receptor ligands: history and perspectives. *Med. Res. Rev.* **2000,** 20, 103-128.

14.   Baraldi, P. G.; Preti, D.; Borea, P. A.; Varani, K. Medicinal chemistry of A3 adenosine receptor modulators: pharmacological activities and therapeutic implications. *J. Med. Chem.* **2012,** 55, 5676-5703.

15.   Hasko, G.; Linden, J.; Cronstein, B.; Pacher, P. Adenosine receptors: therapeutic aspects for inflammatory and immune diseases. *Nat. Rev. Drug Discov.* **2008,** 7, 759-770.

16.   Guo, D.; Hillger, J. M.; IJzerman, A. P.; Heitman, L. H. Drug-target residence time—a case for G protein-coupled receptors. *Med. Res. Rev.* **2014,** 34, 856-892.

17.   Cusack, K. P.; Wang, Y.; Hoemann, M. Z.; Marjanovic, J.; Heym, R. G.; Vasudevan, A. Design strategies to address kinetics of drug binding and residence time. *Bioorg. Med. Chem. Lett.* **2015,** 25, 2019-2027.

18.   Copeland, R. A.; Pompliano, D. L.; Meek, T. D. Drug-target residence time and its implications for lead optimization. *Nat. Rev. Drug Discov.* **2006,** 5, 730-739.

19.   Copeland, R. A. The drug-target residence time model: a 10-year retrospective. *Nat. Rev. Drug Discov.* **2016,** 15, 87-95.

20.   Zeilinger, M.; Pichler, F.; Nics, L.; Wadsak, W.; Spreitzer, H.; Hacker, M.; Mitterhauser, M. New approaches for the reliable in vitro assessment of binding affinity based on high-resolution real-time data acquisition of radioligand-receptor binding kinetics. *EJNMMI Research* **2017,** 7, 22.

21.   Guo, D.; Heitman, L. H.; IJzerman, A. P. Kinetic aspects of the interaction between ligand and G protein-coupled receptor: the case of the adenosine receptors. *Chem. Rev.* **2017,** 117, 38-66.

22.   Topliss, J. G. A manual method for applying the Hansch approach to drug design. *J. Med. Chem.* **1977,** 20, 463-469.

23.   Priego, E.-M.; Pérez-Pérez, M.-J.; von Frijtag Drabbe Kuenzel, J. K.; de Vries, H.; IJzerman, A. P.; Camarasa, M.-J.; Martín-Santamaría, S. Selective human adenosine A3 antagonists based on pyrido[2,1-f]purine-2,4-diones: novel features of hA3 antagonist binding. *ChemMedChem* **2008,** 3, 111-119.

24.   Priego, E.-M.; von Frijtag Drabbe Kuenzel, J.; IJzerman, A. P.; Camarasa, M.-J.; Pérez-Pérez, M.-J. Pyrido[2,1-f]purine-2,4-dione derivatives as a novel class of highly potent human A3 adenosine receptor antagonists. *J. Med. Chem.* **2002,** 45, 3337-3344.

25.   Kalla, R.; Perry, T.; Elzein, E.; Varkhedkar, V.; Li, X.; Ibrahim, P.; Palle, V.; Xiao, D.; Zablocki, J. Xanthine derivatives as a2b adenosine receptor antagonists. WO2004106337 A1, 2004.

26.   Müller, C. E.; Diekmann, M.; Thorand, M.; Ozola, V. [3H]8-Ethyl-4-methyl-2-phenyl-(8R)-4,5,7,8-tetrahydro-1H-imidazo[2,1-i]-purin-5-one ([3H]PSB-11), a novel high-affinity antagonist radioligand for human A3 adenosine receptors. *Bioorg. Med. Chem. Lett.* **2002,** 12, 501-503.

27.   Guo, D.; van Dorp, E. J. H.; Mulder-Krieger, T.; van Veldhoven, J. P. D.; Brussee, J.; IJzerman, A. P.; Heitman, L. H. Dual-point competition association assay: a fast and high-throughput kinetic screening method for assessing ligand-receptor binding kinetics. *J. Biomol. Screening* **2013,** 18, 309-320.

28.   Vauquelin, G. Cell membranes… and how long drugs may exert beneficial pharmacological activity in vivo. *Br. J. Clin. Pharmacol.* **2016,** 82, 673-682.

29.   Hu, M.-H.; Chen, X.; Chen, S.-B.; Ou, T.-M.; Yao, M.; Gu, L.-Q.; Huang, Z.-S.; Tan, J.-H. A new application of click chemistry in situ: development of fluorescent probe for specific G-quadruplex topology. *Sci. Rep.* **2015,** 5, 17202.

30.   Kolb, H. C.; Sharpless, K. B. The growing impact of click chemistry on drug discovery. *Drug Discovery Today* **2003,** 8, 1128-1137.

31.   Tian, H.; Fürstenberg, A.; Huber, T. Labeling and single-molecule methods yo monitor G protein-coupled receptor dynamics. *Chem. Rev.* **2017,** 117, 186-245.

32.   Tummino, P. J.; Copeland, R. A. Residence time of receptor–ligand complexes and Its Effect on Biological Function. *Biochemistry* **2008,** 47, 5481-5492.

33.   Smith, G. F. Medicinal chemistry by the numbers: the physicochemistry, thermodynamics and kinetics of modern drug design. In *Prog. Med. Chem.*, Lawton, G.; Witty, D. R., Eds. Elsevier B.V.: Burlington, **2009**; Vol. 48, p 1.

34.   Wilcken, R.; Zimmermann, M. O.; Lange, A.; Joerger, A. C.; Boeckler, F. M. Principles and applications of halogen bonding in medicinal chemistry and chemical biology. *J. Med. Chem.* **2013,** 56, 1363-1388.

35.   Markgren, P.-O.; Schaal, W.; Hämäläinen, M.; Karlén, A.; Hallberg, A.; Samuelsson, B.; Danielson, U. H. Relationships between structure and interaction kinetics for HIV-1 protease inhibitors. *J. Med. Chem.* **2002,** 45, 5430-5439.

36.   Yu, Z.; van Veldhoven, J. P. D.; Louvel, J.; 't Hart, I. M. E.; Rook, M. B.; van der Heyden, M. A. G.; Heitman, L. H.; IJzerman, A. P. Structure–affinity relationships (SARs) and structure–kinetics relationships (SKRs) of Kv11.1 blockers. *J. Med. Chem.* **2015,** 58, 5916-5929.

37.   Polosa, R.; Blackburn, M. R. Adenosine receptors as targets for therapeutic intervention in asthma and chronic obstructive pulmonary disease. *Trends Pharmacol. Sci.* **2009,** 30, 528-535.

38.   Barnes, P. J. The role of anticholinergics in chronic obstructive pulmonary disease. *Am. J. Med. Supplements* **2004,** 117, 24-32.

39.   Tashkin, D. P. Is a long-acting inhaled bronchodilator the first agent to use in stable chronic obstructive pulmonary disease? *Curr. Opin. Pulm. Med.* **2005,** 11, 121-128.

40.   Cazzola, M.; Page, C. Long-acting bronchodilators in COPD: where are we now and where are we going? *Breathe* **2014,** 10, 110-120.

41.   Liu, W.; Chun, E.; Thompson, A. A.; Chubukov, P.; Xu, F.; Katritch, V.; Han, G. W.; Roth, C. B.; Heitman, L. H.; IJzerman, A. P. Structural basis for allosteric regulation of GPCRs by sodium ions. *Science* **2012,** 337, 232-236.

42.   Abel, R.; Young, T.; Farid, R.; Berne, B. J.; Friesner, R. A. Role of the active-site solvent in the thermodynamics of factor Xa ligand binding. *J. Am. Chem. Soc.* **2008,** 130, 2817-2831.

43.   Young, T.; Abel, R.; Kim, B.; Berne, B. J.; Friesner, R. A. Motifs for molecular recognition exploiting hydrophobic enclosure in protein–ligand binding. *Proc. Natl. Acad. Sci. U. S. A.* **2007,** 104, 808-813.

44.   Heitman, L. H.; Göblyös, A.; Zweemer, A. M.; Bakker, R.; Mulder-Krieger, T.; van Veldhoven, J. P. D.; de Vries, H.; Brussee, J.; IJzerman, A. P. A Series of 2,4-disubstituted quinolines as a new class of allosteric enhancers of the adenosine A3 receptor. *J. Med. Chem.* **2009,** 52, 926-931.

45.   Smith, P. K.; Krohn, R. I.; Hermanson, G. T.; Mallia, A. K.; Gartner, F. H.; Provenzano, M. D.; Fujimoto, E. K.; Goeke, N. M.; Olson, B. J.; Klenk, D. C. Measurement of protein using bicinchoninic acid. *Anal. Biochem.* **1985,** 150, 76-85.

46.   Motulsky, H. J.; Mahan, L. C. The kinetics of competitive radioligand binding predicted by the law of mass action. *Mol. Pharmacol.* **1984,** 25, 1-9.

47.   Cheng, Y.-C.; Prusoff, W. H. Relationship between the inhibition constant (K_i) and the concentration of inhibitor which causes 50 percent inhibition (IC_{50}) of an enzymatic reaction. *Biochem. Pharmacol.* **1973,** 22, 3099-3108.

48.   Louvel, J.; Guo, D.; Soethoudt, M.; Mocking, T. A.; Lenselink, E. B.; Mulder-Krieger, T.; Heitman, L. H.; IJzerman, A. P. Structure-kinetics relationships of Capadenoson derivatives as adenosine A 1 receptor agonists. *Eur. J. Med. Chem.* **2015,** 101, 681-691.

49.   Isberg, V.; Mordalski, S.; Munk, C.; Rataj, K.; Harpsøe, K.; Hauser, A. S.; Vroling, B.; Bojarski, A. J.; Vriend, G.; Gloriam, D. E. GPCRdb: an information system for G protein-coupled receptors. *Nucleic Acids Res.* **2016,** 44, D356-D364.

50.   Munk, C.; Isberg, V.; Mordalski, S.; Harpsøe, K.; Rataj, K.; Hauser, A.; Kolb, P.; Bojarski, A.; Vriend, G.; Gloriam, D. GPCRdb: the G protein-coupled receptor database–an introduction. *Br. J. Pharmacol.* **2016,** 173, 2195-2207.

51.   Schrödinger, L. L. C., New York. *Schrödinger Release 2016-3: Prime*, 2016.

52.   Jacobson, M. P.; Friesner, R. A.; Xiang, Z.; Honig, B. On the role of the crystal environment in determining protein side-chain conformations. *J. Mol. Biol.* **2002,** 320, 597-608.

53.   Jacobson, M. P.; Pincus, D. L.; Rapp, C. S.; Day, T. J.; Honig, B.; Shaw, D. E.; Friesner, R. A. A hierarchical approach to all-atom protein loop prediction. *Proteins: Struct., Funct., Bioinf.* **2004,** 55, 351-367.

54.   Gaulton, A.; Bellis, L. J.; Bento, A. P.; Chambers, J.; Davies, M.; Hersey, A.; Light, Y.; McGlinchey, S.; Michalovich, D.; Al-Lazikani, B. ChEMBL: a large-scale bioactivity database for drug discovery. *Nucleic Acids Res.* **2012,** 40, D1100-D1107.

55.   Accelrys Software Inc. *Pipeline pilot version 9.2*, Scitegic: 2016.

56.   Mysinger, M. M.; Carchia, M.; Irwin, J. J.; Shoichet, B. K. Directory of useful decoys, enhanced (DUD-E): better ligands and decoys for better benchmarking. *J. Med. Chem.* **2012,** 55, 6582-6594.

57.   Sherman, W.; Day, T.; Jacobson, M. P.; Friesner, R. A.; Farid, R. Novel procedure for modeling ligand/receptor induced fit effects. *J. Med. Chem.* **2006,** 49, 534-553.

58.   Schrödinger, L. L. C., New York. *The PyMOL molecular graphics system, version 1.8* 2016.

Supporting information

The binding affinities of short RT antagonist (**5**) and long RT antagonist (**27**) at human adenosine A_1 and A_{2A} receptors, the KRI values of pyrido[2,1-f]purine-2,4- dione derivatives without methoxy-substitution at C-8 position, the comparison with their methoxy-substituted counterparts, and the correlation between pkoff and Log P of the compounds.

1. Binding affinities of short RT antagonist (**5**) and long RT antagonist (**27**) at human adenosine A_1 and A_{2A} receptors.

Binding affinities of antagonist **5** at hA_1 and hA_{2A} receptors have been reported before,[1] whilst binding affinities of antagonist **27** at hA_1 and hA_{2A} receptors were determined as described previously.[2,3] Percentage displacement of antagonists (n=2, average) or $K_i \pm$ SEM (nM, n=3) at human adenosine A_1 and A_{2A} receptors are listed in **Table S1**.

Table S1. Binding affinities of short RT antagonist (**5**) and long RT antagonist (**27**) at human adenosine A_1 and A_{2A} receptors.

Compound	hA_1 [a]	hA_{2A} [b]
5	49%[c]	10%[c]
27	209 ± 16	24%

[a] Displacement of [^{3}H]DPCPX from CHO cell membranes expressing the human adenosine A_1 receptor. Percentage displacement at 10 µM (n=2, average) or $K_i \pm$ SEM (nM, n=3).

[b] Displacement of [^{3}H]ZM241385 from HEK_{293} cell membranes expressing the human adenosine A_{2A} receptor. Percentage displacement at 10 (**5**) or 1 µM (**27**, n=2, average),

[c] Published data.[1]

2. The KRI values of pyrido[2,1-f]purine-2,4-dione derivatives without methoxy-substitution at C-8 position.

157

The KRI values of pyrido[2,1-f]purine-2,4-dione derivatives without methoxy-substitution at C-8 position were obtained as described under "*the 'dual-point' competition association assays*". Experiments were designed as described previously,[4] where in this case the two time points were selected at 20 (t_1) and 240 min (t_2). The results are listed in **Table S2**.

Table S2. Kinetic Parameters of Pyrido[2,1-*f*]purine-2,4-dione Derivatives without Methoxy-substitution at *C*-8 Position.
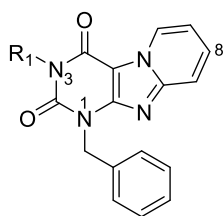
Compound	R_1	KRI[a]
S1	CH_2CH_3	0.61 (0.63,0.59)
S2	$CH_2CH_2CH_3$	0.59 (0.40,0.77)
S3	$CH_2CH(CH_3)_2$	0.88 (0.85,0.90)
S4	$CH_2CH=CH_2$	0.88 (0.79,0.96)
S5	$CH_2C≡CH$	1.16 ± 0.38
S6	$CH_2C_3H_5$	1.01 (1.08,0.93)

[a] KRI ± SEM (n = 3) or KRI (n = 2, individual estimates in parentheses), obtained at 10 °C from dual point competition association assays at 10 °C with [^{3}H]**34** on CHO cell membranes stably expressing the hA$_3$R.

3. The comparison between the KRI values of pyrido[2,1-f]purine-2,4-dione derivatives without methoxy-substitution at C-8 position and their methoxy-substituted counterparts The comparison is presented in **Figure S1**.
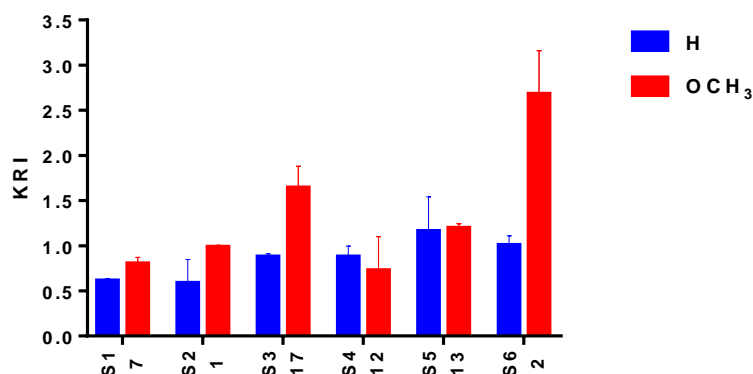

Figure S1: Comparison of KRI values of compounds with (red bars) and without (blue bars) *C*-8 methoxy substitution. KRI values obtained from dual point competition association assay on CHO cells stably expressing hA$_3$R at 10 °C. Each data point is the average of two or three independent experiments performed in duplicate.

4. The correlation between pk_{off} and LogP for antagonists.

Log*P* values were calculated using Chemdraw Professional 15.0 (Cambridge Soft, Perkin Elmer, Waltham, MA, USA). R^2 and *P* values were calculated using the GraphPad Prism linear regression analysis function. The correlations are presented in **Figure S2**.
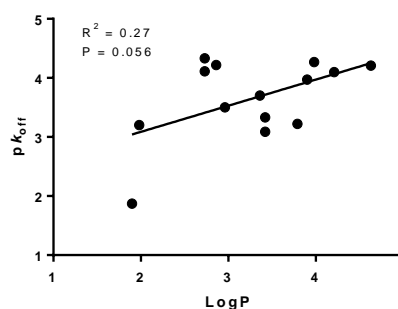
A.
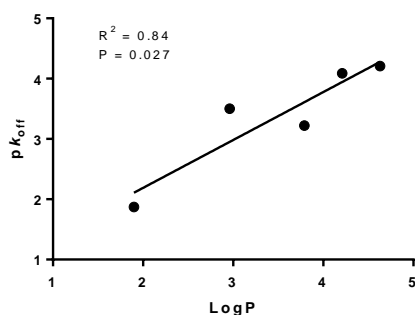
B.

Figure S2: Correlation between pk_{off} and LogP for antagonists with an elongated carbon chain (**1, 5, 9, 10** and **11**) at the R$_1$ position (A), or for all antagonists (B), obtained from competition association assays.

References

1.   Priego, E.-M.; von Frijtag Drabbe Kuenzel, J.; IJzerman, A. P.; Camarasa, M.-J.; Pérez-Pérez, M.-J. Pyrido[2,1-f]purine-2,4-dione derivatives as a novel class of highly potent human A3 adenosine receptor antagonists. *J. Med. Chem.* **2002,** *45*, 3337-3344.

2.   Guo, D.; Xia, L.; van Veldhoven, J. P. D.; Hazeu, M.; Mocking, T.; Brussee, J.; IJzerman, A. P.; Heitman, L. H. Binding Kinetics of ZM241385 Derivatives at the human adenosine A_{2A} receptor. *ChemMedChem* **2014,** *9*, 752-761.

3.   Xia, L.; de Vries, H.; IJzerman, A. P.; Heitman, L. H. Scintillation proximity assay (SPA) as a new approach to determine a ligand's kinetic profile. A case in point for the adenosine A_1 receptor. *Purinergic Signalling* **2016,** *12*, 115-126.

4.   Guo, D.; van Dorp, E. J. H.; Mulder-Krieger, T.; van Veldhoven, J. P. D.; Brussee, J.; IJzerman, A. P.; Heitman, L. H. Dual-point competition association assay: a fast and high-throughput kinetic screening method for assessing ligand-receptor binding kinetics. *J. Biomol. Screening* **2013,** *18*, 309-320.